CERTIFICATION OF APPROVAL

IMPROVEMENT STUDY ON SOFT-SWITCHED QUASI-RESONANT DC/DC BOOST CONVERTER

by

Tran Minh Dung

A project dissertation submitted to the
Electrical & Electronics Engineering Programme
Universiti Teknologi PETRONAS
in partial fulfilment of the requirement for the
Bachelor of Engineering (Hons)
(Electrical & Electronics Engineering)

Approved:

_____
Mr. Nor Zaihar Yahaya
Project Supervisor

Nor Zaihar Bin Yahaya
Lecturer,
Electrical & Electronic Engineering
Academic Block No 22, Level 3, Room 4
Universiti Teknologi PETRONAS
Bandar Seri Iskandar
31750 Tronoh, Perak Darul Ridzuan, MALAYSIA

UNIVERSITI TEKNOLOGI PETRONAS
TRONOH, PERAK

December 2006

CERTIFICATION OF ORIGINALITY

This is to certify that I am responsible for the work submitted in this project, that the original work is my own except as specified in references and acknowledgements and that the original works contained herein have not been undertaken or done by unspecified sources or persons.

Tran Minh Dung

ABSTRACT

This report describes a novel soft-switched quasi-resonant DC/DC boost converter. Recently, remarkable efforts have been made in soft-switched quasi-resonant DC/DC converters to reduce losses and improve power efficiency. This project presents a new technique and it had improved the performance of the most recent study on soft-switched quasi-resonant DC/DC boost converter, which is presented in Ba-Thunya and Prasad's study [1]. The proposed converter employs an active snubber circuit with an auxiliary switch in series with a clamp capacitor to reduce power losses in Ba-Thunya and Prasad's original an active snubber circuit with an auxiliary switch and a clamp diode to reduce power losses in Ba-Thunya and Prasad's original converter. The energy from the snubber inductor after the auxiliary switch turn-off is returned to the input or delivered to the output via the active snubber circuit, thus the voltage stress on the main switch is reduced and switching losses are minimized. Furthermore, the proposed converter reduces the reverse-recovery-related losses of the boost rectifier by controlling the di/dt rate of the rectifier current with the snubber inductor. This report describes the principle of operation of the new soft-switched quasi-resonant DC/DC boost converter. The feasibility study of the proposed converter is investigated using PSPICE program.

ACKNOWLEDGEMENTS

TABLE OF CONTENTS

LIST OF TABLES

LIST OF FIGURES

LIST OF ABBREVIATIONS

AC	Alternating Current
D	Duty Ratio
DC	Direct Current
EMI	Electromagnetic Interference
EV	Electric Vehicle
HEV	Hybrid Electric Vehicle
MOSFET	Metal-Oxide-Semiconductor Field-Effect-Transistor
PCB	Printed Board Circuit
PWM	Pulse Width Modulation
SEPIC	Single Ended Primary Inductor Converter
ZCS	Zero Current Switching
ZVS	Zero Voltage Switching

CHAPTER 1

INTRODUCTION

1.1 Background of Study

In recent years, significant research and development efforts have been made in soft-switched quasi-resonant DC/DC converters to reduce losses and to increase the switching frequency. Soft-switched quasi-resonant DC/DC converters having increased efficiency, low cost, high power operation and reduced weight as well as size have been produced to give applications in industry such as high-power high-efficiency power supplies, direct-current motor drives electric vehicles (EV) and hybrid electric vehicles (HEV) systems.

The project is about designing and implementing a new quasi-resonant soft-switched DC/DC boost converter. The original circuit was selected from the most recent and suitable study on the subject in power electronic field. The proposed quasi-resonant soft-switched DC/DC boost converter has improvements over the original circuit presented in Ba-Thunya and Prasad's study. The proposed design's feasibility is verified by PSPICE simulation. Throughout the project, the knowledge about DC/DC converters, quasi-resonant boost converters, analog and power electronics will be applied.

1.2 Problem Statement

The major thrust in soft-switched quasi-resonant DC/DC boost converter improvement study is to reduce losses and to increase the switching frequency. The current proposed circuit of Ba-Thunya and Prasad's study, which use two coupled inductors with capacitor for the resonant circuit (shown in **Figure 1**) [1] provides a valuable solution to achieve high switching frequency, and allow zero voltage and zero current switching for turning

1

off the control switch and zero current switching for turning it on. The main drawback of this converter is the voltage stresses on the control switch and boost rectifier.

Furthermore, at high output voltage, the converter requires the use of a fast-recovery boost rectifier. At high switching frequencies, fast-recovery rectifiers produce significant reverse-recovery-related losses when switched under "hard-switched" conditions [2], this leads to high total power loss and low power efficiency. This project focuses on modifying the soft-switched quasi-resonant DC/DC boost converter by using an active snubber circuit consisting of an auxiliary switch in series with a clamp capacitor [3], [4]. In addition, a clamp diode is connected between the ground and the anode of the snubber diode, which is in series with the boost rectifier. The energy from the snubber inductor after the switch turn-off is returned to the input or delivered to the output via the active snubber circuit, thus reduces the voltage stress on the main switch and reduces the switching loss. Furthermore, the clamp diode effect is to eliminate the parasitic ringing between the junction capacitance of the rectifier and the snubber inductor, the stress of the rectifier is therefore minimized.
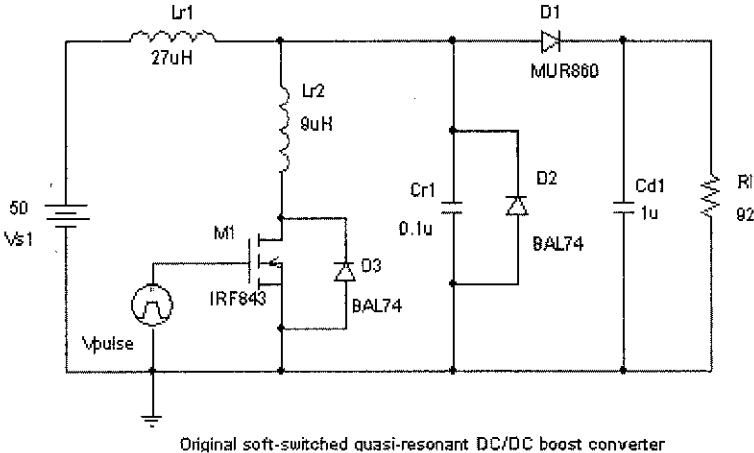
Original soft-switched quasi-resonant DC/DC boost converter

Figure 1: Original quasi-resonant soft-switched DC/DC boost converter using two coupled inductors with capacitor

1.3 Objectives and Scope of Study

1.3.1 Objectives

The objectives of the project are:

1. To design an active snubber circuit consisting of an auxiliary switch in series with a clamp capacitor to improve the performance of the most recent study of soft-switched quasi-resonant DC/DC boost converter (Ba-Thunya and Prasad's study).
2. To do simulation on the selected design.

1.3.2 Scope of Study

The study consists of designing, simulating a modified soft-switched quasi-resonant DC/DC boost converter with an active snubber circuit in order to achieve the objectives. In addition, the study also includes evaluation on the performance of the proposed design. The evaluation focuses on power efficiency, output ripple voltage and the main switch performance.

CHAPTER 2

LITERATURE REVIEW

2.1 Basic Study Concepts

The study is about improvement of soft-switching quasi-resonant DC/DC converter. The study is related with the concepts of conventional boost converter, resonant converter, quasi-resonant switch, quasi-resonant converter and snubber networks.

Basically, the DC/DC boost converter provides a DC output voltage that is greater than the DC input voltage and DC output current is less than DC input current. It is also known as "ringing choke", a current step-down DC/DC converter or a voltage step-up DC/DC converter. A soft-switching DC/DC boost converter is a DC/DC boost converter with the soft-switching characteristic, which are either the turn-on or turn-off switching losses eliminated. The soft-switching quasi-resonant DC/DC boost converter is a DC/DC boost converter which employs an LC tank circuit to shape the current or voltage waveform of the switching transistor resulting in a zero-current switching (ZCS) or zero-voltage switching (ZVS) condition during boost converter turn-off or turn-on.

Followings are the detailed explanations of concepts related to the project, including conventional boost converter, resonant converter, quasi-resonant switch and quasi-resonant converter.

4

2.1.1 Conventional boost converter

The conventional boost converter shown in **Figure 2** below:
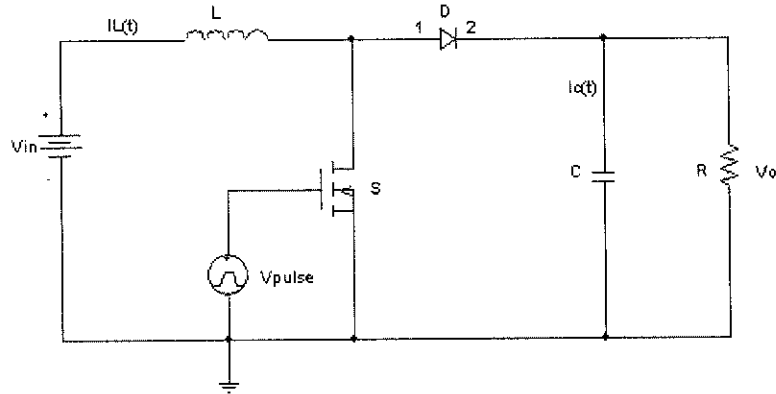
Figure 2: Conventional Boost DC/DC converter circuit

During the time when the switch is closed, energy is transferred to the inductor while the diode is preventing the capacitor to discharge through the switch. When the switch opens, current through the inductor continues to flow in the same direction as during the previous cycle. This forward-biases the diode and both the input voltage source and the inductor are transferring energy to the load. Hence, a voltage boost occurs across the load, which causes the output voltage to be higher than the input voltage. The capacitor must be large enough to keep the output voltage approximately constant [5].

The operation of the basic boost converter can be divided into two modes: continuous and discontinuous mode. In this study, we mainly focus on the continuous mode of the converter.
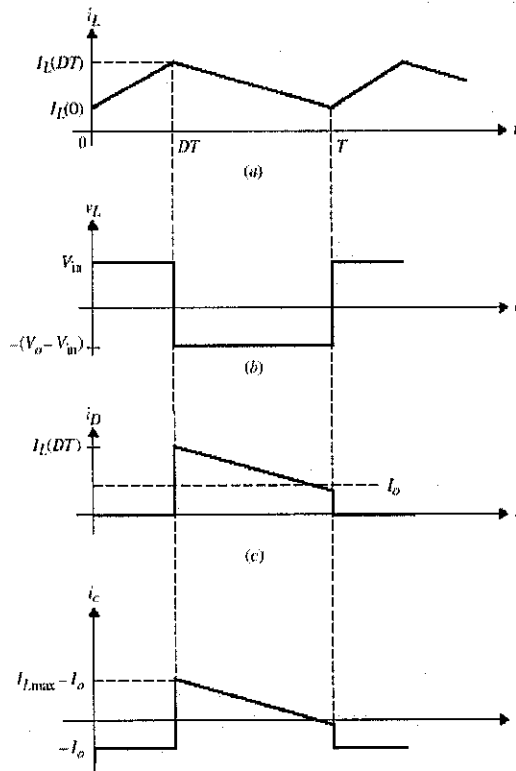
Figure 3: Voltage and Current waveforms for the boost converter.

Mode 1 $(0<t\le t_{on})$:
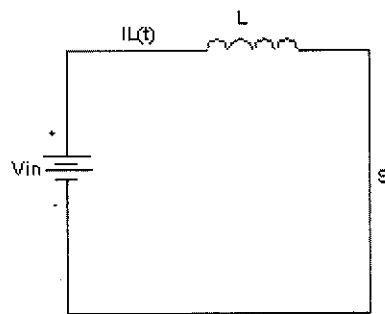
Figure 4: Mode 1 equivalent circuit for the boost converter $(0<t\le t_{on})$

Mode 1 begins when the switching transistor, S, is switched on at $t = 0$ and it terminates at $t = t_{on}$. The equivalent circuit for Mode 1 is shown in **Figure 4**. The diode S is reverse biased since the voltage drop across the collector-emitter junction of the switching transistor is smaller than the output voltage. The inductor current, $i_L(t)$, ramps up linearly from $I_L(0)$ to $I_L(DT)$ in time t_{on} so that:

6

$$V_{in} = L\frac{I_L(DT) - I_L(0)}{t_{on}} = L\frac{\Delta I}{t_{on}}$$

The duration of the interval t_{on} can be expressed as:

$$t_{on} = \frac{L\Delta I}{V_s}$$

The energy stored in the inductor is:

$$E = \frac{1}{2}L(\Delta I)^2 = \frac{1}{2L}V_s^2 t^2_{on}$$

The output current during this interval is supplied entirely from the output capacitor, C, which is chosen large enough to supply the load current during t_{on} with a minimum specified droop in output current.

Mode 2 $(t_{on} < t \leq T)$:
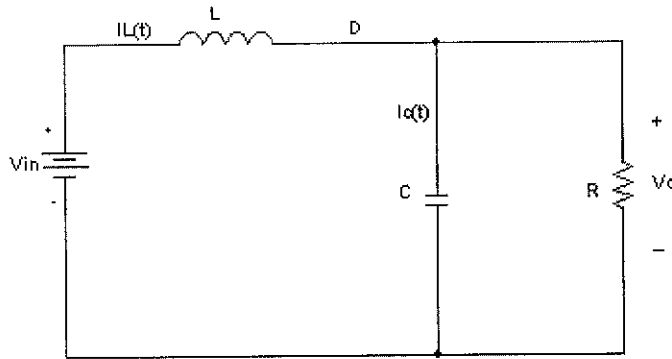
Figure 5: Mode 2 equivalent circuit for the boost converter $(t_{on} < t \leq T)$

Mode 2 begins when the switching transistor, S, is switched off at $t = t_{on}$. The equivalent circuit for this mode is shown in **Figure 5**. Since the current in the inductor cannot change instantaneously, the voltage in the inductor reserves its polarity in an attempt to maintain a constant current. The current which was flowing through the switching transistor will not flow through L, C, D, and the load. The inductor current decreases until the switching transistor is turned on again during the next cycle. The inductor delivers its stored energy to the output capacitor, C, and charges it up via D to a higher voltage than the input voltage V_{in}. The energy supplies the current and replenishes the charge drained away from the output capacitor when it alone was supplying the load current during the

on time. The voltage across the inductor is $V_o\text{-}V_{in}$ and the inductor current decreases linearly from $I_L(DT)$ to $I_L(0)$ in time t_{off}.

$$V_o - V_{in} = L\frac{I_L(DT) - I_L(T)}{t_{off}} \qquad (1)$$

The duration of the interval t_{off} can then be expressed as:

$$t_{off} = \frac{L\Delta I}{V_o - V_{in}} \qquad (2)$$

Since the change in the peak-to-peak inductor ripple current, ΔI, is the same during t_{on} and t_{off} for steady state operation, it can be shown from equations (1) and (2) that:

$$\Delta I = \frac{V_{in}t_{on}}{L} = \frac{(V_o - V_{in})t_{off}}{L} \qquad (3)$$

Substituting $t_{on}=DT$ and $t_{off}=(1-D)T$ into equation (3), we have:

$$V_{in}DT = (V_o\text{-}V_{in})(1\text{-}D)T = V_o(1\text{-}D)T - V_{in}(1\text{-}D)T$$

Simplifying the above equation, we get:

$$V_{in}DT = V_o(1\text{-}D)T - V_{in}T + V_{in}DT$$

$$\text{or} \quad V_{in} = V_o(1\text{-}D)$$

The average output voltage, V_o, for a boost converter is:

$$V_o = \frac{V_{in}}{1-D}$$

Thus, V_o is inversely proportional to $1\text{-}D$. Assuming a lossless boost converter, then:

$$V_{in}I_{in} = V_oI_o = \frac{V_{in}I_o}{1-D}$$

The average input current, I_{in}, can be expressed as:

$$I_{in} = \frac{I_o}{1-D}$$

Then, the average output current, I_o, is reduced by a factor of $(1\text{-}D)$ from the average input current since the output power can only be, at best, equal to the input power. The switching period, T, is the sum of t_{on} and t_{off}:

$$T = \frac{1}{f_s} = t_{on} + t_{off} = \frac{L\Delta I}{V_{in}} + \frac{L\Delta I}{V_o - V_{in}} = \frac{(\Delta I)LV_o}{V_{in}(V_o - V_{in})}$$

The peak-to-peak inductor ripple current, ΔI, is:

8

$$\Delta I = \frac{V_{in}(V_o - V_{in})}{LV_o} = \frac{V_{in}(V_{in}/(1-D) - V_{in})}{f_s LV_o}$$

Simplifying the equation, we have:

$$\Delta I = \frac{V_{in}D}{f_s L}$$

The magnitude of ΔI is inversely proportional to f_s and L.
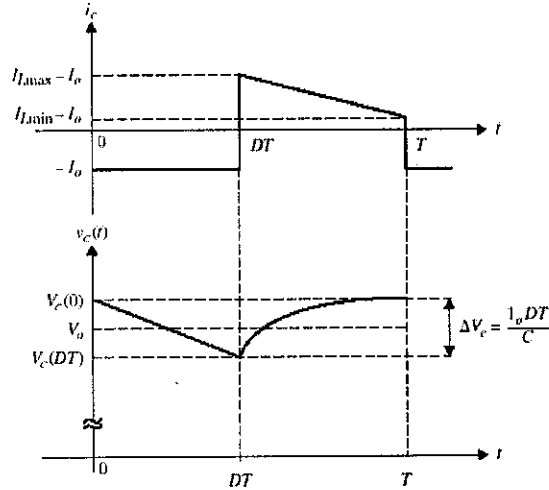
Figure 6: Capacitor voltage and current waveforms of basic DC/DC boost converter.

When the switching transistor, S, is switched on, the capacitor supplies the load current for the entire time. Thus, the average capacitor current, I_c, is equal to the equal to the average output current, I_o, during this interval. During the off-time the output capacitor is being charged. The capacitor charging current, decreases linearly from an initial value of $I_{Lmax}-I_o$ to a final value of $I_{Lmin}-I_o$, as shown in **Figure 6**. For steady-state operation, the average capacitor charging current-time product during the off-time interval must be equal to the average capacitor discharging current –time product during the only the on-time interval. The peak-to-peak capacitor ripple voltage can be found by recognizing that the average output current, I_o. Thus:

$$\Delta v_c = v_c - v_c(0) = \frac{1}{C}\int_0^{t_{on}} I_o dt = \frac{I_o t_{on}}{C} \qquad (4)$$

The t_{on} can be expressed in terms of the input voltage, switching frequency, and average output voltage:

9

$$V_o = \frac{V_{in}}{1-D} = \frac{V_{in}T}{T-DT} = \frac{V_{in}T}{T-t_{on}}$$

$$\text{or} \quad T - t_{on} = \frac{V_{in}T}{V_o}$$

$$t_{on} = T - \frac{V_{in}T}{V_o} = \frac{V_o - V_{in}}{f_s V_o} \tag{5}$$

Substituting equation (5) into equation (4):

$$v_c = \frac{I_o(V_o - V_{in})}{V_o f_{in} C} = \frac{I_o(V_o - V_{in})}{f_s C V_{in}/(1-D)}$$

Simplifying the above equation, we have:

$$\Delta v_c = \frac{I_o[(V_{in} - V_{in} + DV_{in})/(1-D)]}{f_s C V_{in}(1-D)} = \frac{I_o D}{f_s C}$$

The peak-to-peak output ripple voltage, Δv_o, is equal to the peak-to-peak capacitor ripple voltage, Δv_c. It is evident that Δv_o can be reduced by increasing either the switching frequency or the capacitance of the output capacitor [6].

2.1.2 Resonant converter

The previous topic was about the conventional boost converter or hard–switching boost converter, which employ pulse-width-modulation to control the dynamic transfer of electrical energy from the input to the output. As we know, the major thrusts in the study of improvement of switching converter are to achieve a higher power-packing density and higher conversion efficiency. To increase the power-packing density, the switching frequency of the switching converter is often increased to reduce the size and weight if it's reactive components. However, the conventional / hard-switching converter suffers an excessive switching loss as its switching frequency approaches 1 MHz. The higher the switching losses of the power transistor require a larger heat-sink capacity that offsets the net magnetic size reduction when operating at a higher switching frequency. At high switching frequencies, capacitive turn-on losses in power MOSFETs become the predominant switching losses. For example, a power MOSFET with C_{ds} of 100 pF, switching at 500 V, will have a turn-on loss of $0.5C_{ds}f_s V^2_{ds}$, equals 12.5 W, when

operating at 1 MHz. However, the turn-on loss increases to 62.5 W when this device operates at a switching frequency of 5 MHz. Resonant converters offer an attractive solution to the limitation of conventional boost converter.

Basically, resonant converters are used to convert dc-to-dc through an additional stage: the resonant stage, in which the dc signal is converted to a high-frequency ac signal. the advantages of the resonant converter include the natural commutation of power switches, resulting in low switching power dissipation and reduced component stress, which in turn results in increased power efficiency and increased switching frequency; and higher operating frequencies, resulting in reduced sized and weight of equipment and faster response, and hence a possible reduction in EMI problems [7].
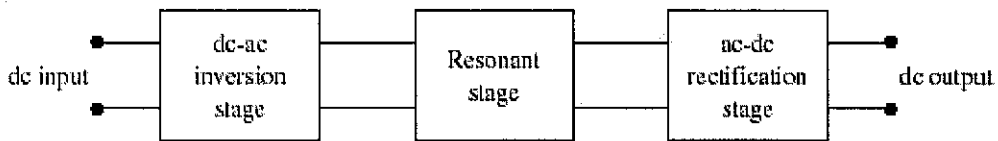
Figure 7: Typical block diagram of soft-switching DC/DC converter

Based on the diagram, we can describe dc-to-dc resonant converter by three major circuit blocks: the dc-to-ac inversion circuit, the resonant energy buffer tank circuit, and the ac-to-dc output rectifying circuit. Typically, the dc-to-ac inversion is achieved by using various type of switching network topologies. The resonant tank, which servers as an energy buffer between the input and the output, is normally synthesized by using a lossless frequency-selective network is to regulate the energy flow from the source to the load. Finally, the ac-to-dc conversion is achieved by incorporating rectifier circuits at the output selection of the converter.

One of the major advantages of the resonant converters is the absorption of the switching transistor capacitance and other parasitic components into the converter topologies. However, the switching transistors in the resonant converters generally have to carry a higher peak current or voltage for the same output power than their counterparts in conventional switching converters. Since resonant converters regulate their output by changing their switching frequencies or by frequency modulation, electro-magnetic

11

interference may be unpredictable. The choice of using resonant converters over conventional switching converters should be based on the fact that the reduction in switching losses is greater than the increase in semiconductor device conduction losses associated with the higher peak current or voltage in the resonant topologies. Before embarking on the quasi-resonant converter, let us have a review of the fundamental concept of parallel and series resonant circuits.

2.1.2.1 Parallel Resonant Circuit

Figure 8 shows a parallel resonant circuit with a current source $\vec{I}_s(j\varpi)$ connected in parallel with a resistor R, a capacitor C, and an inductor L. As the frequency of the current source changes the voltage across terminals a and b is given by:

$$\vec{V}_o(j\omega) = \frac{\vec{I}_s}{1/R + j\omega + 1/j\omega L} = \frac{I_m\angle 0^o}{\sqrt{1/R^2 + (\omega C - 1/\omega L)^2}\angle \tan^{-1}[R(\omega C - 1/\omega L)]}$$

The resonant frequency in this circuit is defined as the frequency at which the impedance seen by the current source is purely resistive. The resonant frequency, ω_n, is then:

$$\omega_n C = \frac{1}{\omega_n L}$$

$$\omega_n = \frac{1}{\sqrt{LC}}$$

At the resonant frequency, the voltage across terminals a and b is:

$$\vec{V}_o(\omega = \omega_n) = V_{m(max)} = I_m$$
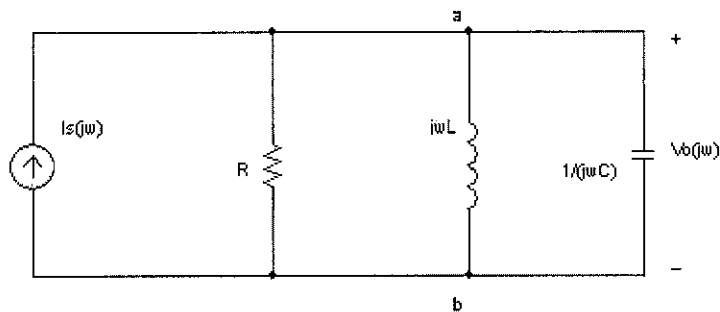
Figure 8: A parallel-resonant circuit

12

2.1.2.2 Series Resonant Circuit

Figure 9 shows a series-resonant circuit with a voltage source $\vec{V}_s(j\omega)$ connected in series with a resistor R, an inductor L, and a capacitor C. As the frequency of the voltage source changes, the current flowing in the circuit is given by:

$$\vec{I} = \frac{\vec{V}_s}{R + j(\omega L - 1/\omega C)} = \frac{\vec{V}_m \angle 0^o}{\sqrt{R^2 + (\omega L - 1/\omega C)} \angle \tan^{-1}\left[\frac{\omega L - 1/\omega C}{R}\right]}$$

Again, the resonant frequency in this circuit is defined as the frequency at which the impedance seen by the voltage source is purely resistive. Thus, the resonant frequency ω_n is given by:

$$\omega_n = \frac{1}{\sqrt{LC}}$$

At the resonant frequency, the current flowing in the circuit is:

$$\vec{I}(\omega = \omega_n) = \vec{I}_{max} = \frac{\vec{V}_m}{R}$$
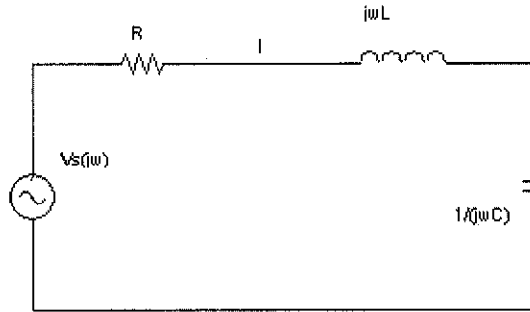
Figure 9: A series-resonant circuit

2.1.3 Quasi-Resonant Switches

As discussed previously, resonant converters introduce a valuable solution about switching losses when switching transistor operates at high frequency. There are many topological variations of the resonant converter. Only quasi-resonant converter is discussed in this study. The quasi-resonant converter employs an LC tank circuit to shape the current or voltage waveform of the switching transistor resulting in a zero-current or

zero-voltage condition during device turn-on or turn-off. This characteristic of quasi-resonant converter is called soft-switching, zero/low loss switching, losses snubbering. To reduce the turn-off switching losses, zero-current-switching quasi-resonant switches are employed. On the other hand, zero-voltage-switching quasi-resonant switches are used to mitigate the turn-on switching losses. In general, zero-voltage-switching is preferable to zero-current-switching at high switching frequencies. In this subtopic, analysis of quasi-resonant switches is explained.

Quasi-resonant switch is basically a conventional semiconductor power-switching device with an LC tank circuit incorporated into a circuit to shape either the voltage across the device or current flowing through it from rectangular pulses into a sinusoidal waveform. There are two-types of quasi-resonant switches are the current mode quasi-resonant switch and the voltage–mode quasi-resonant switch [8], [9]. For the current mode quasi-resonant switch, the inductor of the resonant tank circuit is connected in series with the switching transistor to shape the current flowing through it. **Figure 10** shows two current-mode quasi-resonant switch configurations: the L-type and the M-type.
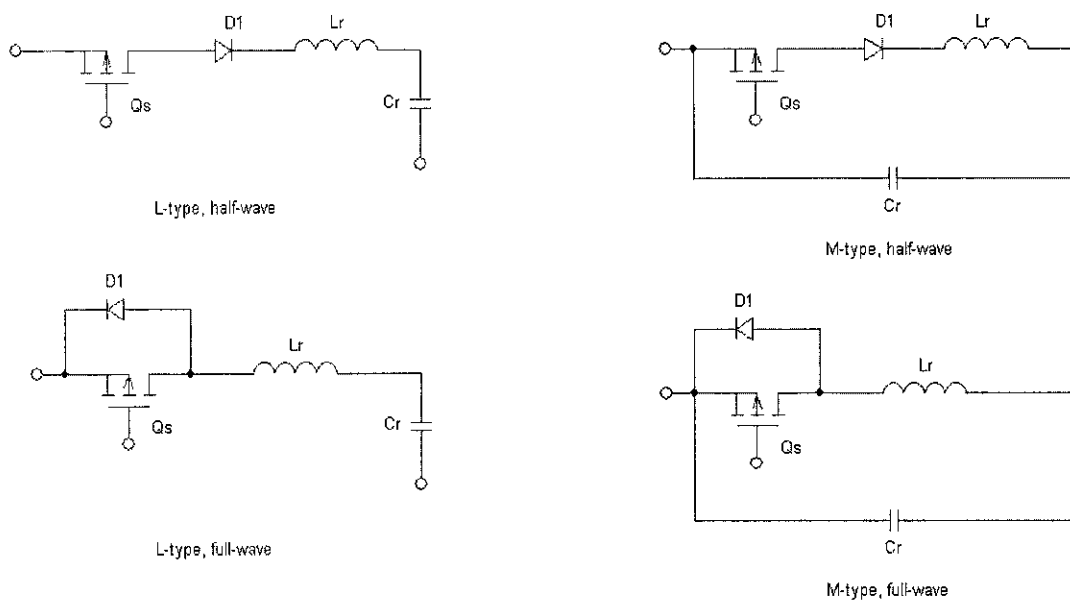
Figure 10: Current-mode quasi-resonant switches

As being seen from two above configurations, the resonant inductor, L_r, is connected in series with the switching transistor, Q_s, while the resonant capacitor, C_r, is connected in

14

parallel with Q_s and L_r. The resonant capacitor and inductor form a series–resonant tank circuit whose resonance occurs during the major portion of the on time of the switching transistor. The quasi-resonant switch operates in a half-wave mode if diode D_l is connected to prevent resonant current from flowing back to the source. If an anti-parallel diode, D_l, is connected across the switching transistor, then the quasi-resonant switch is configured to operate in a full-wave mode and the resonant current can flow bidirectional to both the load and the source.

Figure 11 shows the effect of the resonant switch on the reduction of switching stress and switching losses [10]. Path A shows a typical trajectory for inductive switching of a switching transistor with conventional forced turn-off. It goes through a high-stress region where the switching transistor suffers both high voltage and high current. For load-line trajectory for inductive switching with a current-mode resonant switch is along the voltage axis or the current axis as shown in path B. Consequently, the switching stresses and losses in current-mode quasi-resonant switch are much reduced.
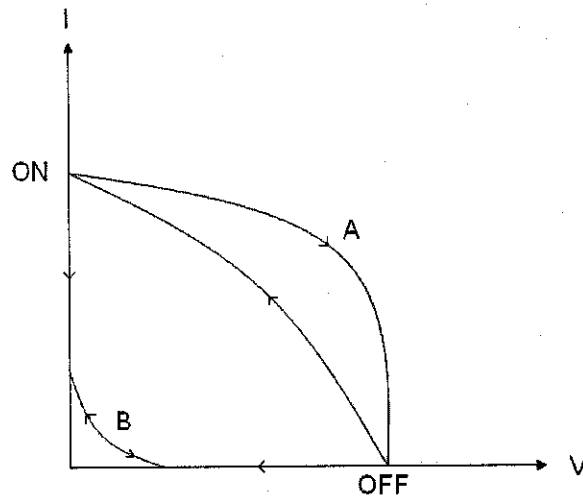
Figure 11: Load-line trajectories of a switching transistor: path A, forced switching; path B, resonant switching.

The voltage-mode quasi-resonant switch is implemented by connecting a resonant capacitor, C_r, in parallel with the switching transistor, Q_s. The purpose is to shape the voltage waveform across the switching transistor during it's OFF time such that a zero-voltage condition created before the device is allowed to switch on. There are two configurations of voltage-mode Quasi-resonant switch: the L-type and the M-type, as

15

shown in **Figure 12**. Like the current-mode quasi-resonant switch, the voltage mode quasi-resonant switch is said to operate in half-wave mode when the voltage across the resonant capacitor is not allowed to swing to its negative cycle (When D_l is connected in parallel with switching transistor). And if the diode D_l is connected in series with the switching transistor, the voltage-mode quasi-resonant switch will operate in full-wave mode since the voltage across the resonant capacitor can swing freely to negative values [11], [12].

L-type, half-wave

M-type, half-wave

L-type, full-wave

M-type, full-wave
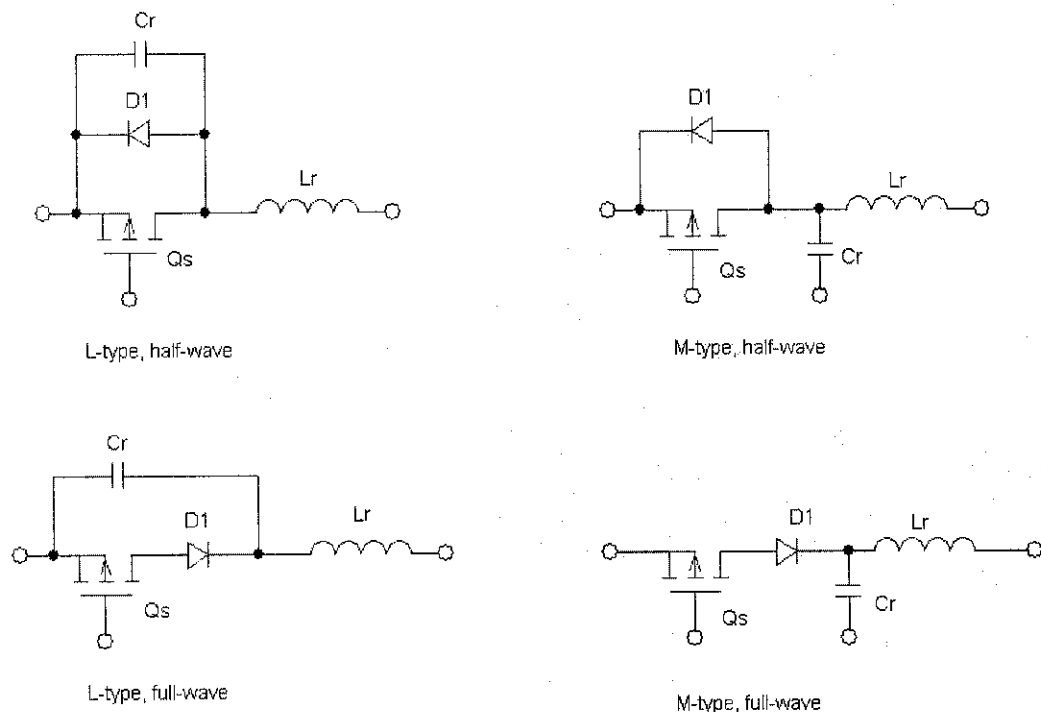
Figure 12: Voltage-mode quasi-resonant switches.

2.1.4 Quasi-Resonant Converter

As mentioned previously, ZCS and ZVS quasi-resonant switches are employed to reduce the turn-off and turn-on switching losses respectively. Basically, a quasi-resonant converter is formed by using a conventional PWM converter-buck, boost, buck-boost, Cuk, SEPIC and replacing the switch with a quasi-resonant switch to accomplish the switching loss elimination [13]. In this context, we only look at quasi-resonant boost converter.

There are 2 types of quasi-resonant boost converters, which are zero-current switching (ZCS) and zero-voltage switching (ZVS) quasi-resonant boost converter. The ZCS quasi-resonant boost converter can be implemented by replacing the switching transistor of the conventional switching boost converter with a current-mode quasi-resonant switch. Similarly, ZVS quasi-resonant boost converter can be implemented by replacing the switching transistor of the conventional switching boost converter with a voltage-mode quasi-resonant switch. Let us review on the operation of ZCS quasi-resonant boost converter and ZVS quasi-resonant boost converter.

2.1.4.1 ZCS Quasi-Resonant Boost Converter

Figure 13 shows the circuit schematic of a full-wave, zero-current-switching (ZCS) quasi-resonant boost converter.
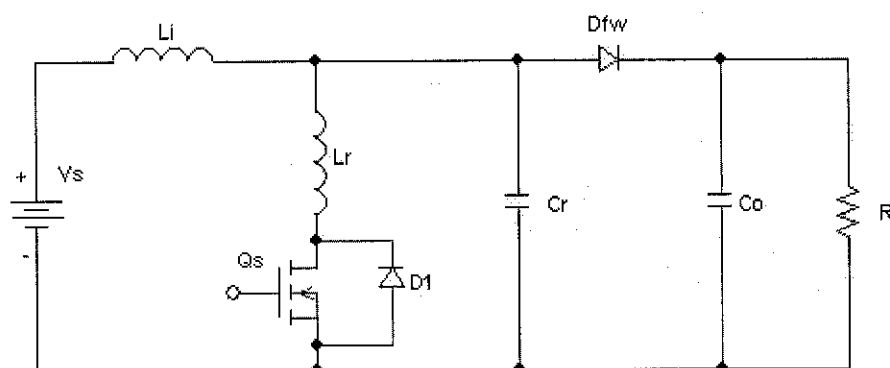
Figure 13: Circuit schematic of a full-wave ZCS quasi-resonant boost converter

The operation of the ZCS quasi-resonant boost converter can also be divided into four modes. Suppose before the switching transistor, Q_s, is switched on, the freewheeling diode is conducting, and, consequently, the resonant capacitor is charged to the output voltage, V_a.

Mode 1 $(0<t\leq t_1)$:
Mode 1 begins when the switching transistor, Q_s, is switched on at $t = 0$. **Figure 14** shows the equivalent circuit. The current flowing through the resonant inductor, $i_{lr}(t)$,

increases linearly from zero to the steady-state input current of I_s. The voltage across the resonant inductor is related to the rate of rise of its current. At the end of mode 1, the voltage across the resonant inductor, $v_{Lr}(t)$, is:

$$V_a = L_r \frac{I_s}{T_1}$$

The duration of mode 1, T_1, is:

$$T_1 = \frac{L_r I_s}{V_a}$$

Thus, mode 1 is characterized by the storage of electrical energy in the resonant inductor in magnetic form.
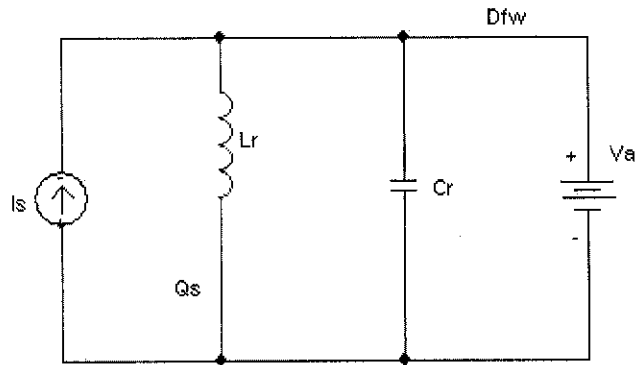
Figure 14: Mode 1 equivalent circuit of the ZCS quasi-resonant boost converter

Mode 2 $(t_1 < t \leq t_2)$:

Mode 2 begins when the current flowing through the resonant inductor reaches the input current, I_s. The freewheeling diode is reverse biased as the resonant capacitor discharges its stored energy to the resonant inductor. The equivalent circuit is shown in **Figure 15**. The voltage across the resonant capacitor, $v_{Cr}(t)$, decreases sinusoidally according to:

$$C_r \frac{dv_{Cr}(t)}{dt} = I_s - i_{Lr}(t)$$

18
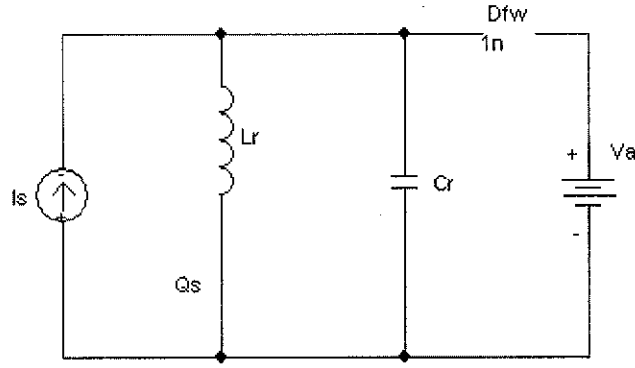
Figure 15: Mode 2 equivalent circuit of the ZCS quasi-resonant boost converter

The rate of the increase of the resonant inductor current, $di_{Lr}(t)/dt$, is:

$$\frac{di_{Lr}(t)}{dt} = \frac{v_{Cr}(t)}{L_r}$$

The preceding first-order differential equations can be solved by using the two known initial conditions: $i_{Lr}(t_1) = i_{Lr}(0) = I_s$ and $v_{Cr}(t_1) = v_{Cr}(0) = V_a$. The expression for $i_{Lr}(t)$ is:

$$i_{Lr}(t) = I_s + \frac{V_a}{Z_n}\sin\omega_n t$$

Where, $Z_n = \sqrt{L_r/C_r}$ is the circuit characteristic impedance and $\omega_n = 1/\sqrt{L_r C_r}$ is the resonant frequency. The expression for $v_{Cr}(t)$ is: $v_{Cr}(t) = V_a\cos\omega_n t$

Thus both the current flowing through the resonant inductor and the voltage across the resonant capacitor is sinusoidal. Hence, electrical energy is exchanged between the resonant inductor and capacitor. Mode 2 is also known as the resonant mode. The resonant inductor current continues to swing to its negative cycle when it feeds energy back to the input source as shown in **Figure 16**. At the beginning of this mode, the resonant capacitor discharges its energy to the resonant inductor. However, as the resonant inductor current decreases below the steady-state input current of I_s, the resonant capacitor voltage increases toward the output voltage, V_a. The duration of this resonant mode, $T_2 = t_2 - t_1$, can be found by setting $i_{Lr}(T_2) = 0$:

$$i_{Lr}(T_2) = 0 = I_s + \frac{V_a}{Z_n}\sin\omega_n T_2$$

19

The duration for mode 2, T_2, is

$$T_2 = \frac{\sin^{-1}(-Z_n I_s / V_a)}{\omega_n} = \frac{\alpha}{\omega_n}$$

(α takes on values between 1.5π and 2π)

The resonant mode terminates at $t_2 = t_b$ after the resonant inductor feeds energy back to the input source. After t_a, the switching transistor, Q_s, can now be switched off. Thus, a zero-current condition is created for the switching transistor to switch off. The input current, I_s, should be smaller than V_a/Z_n for the switching transistor to switch off during zero current.
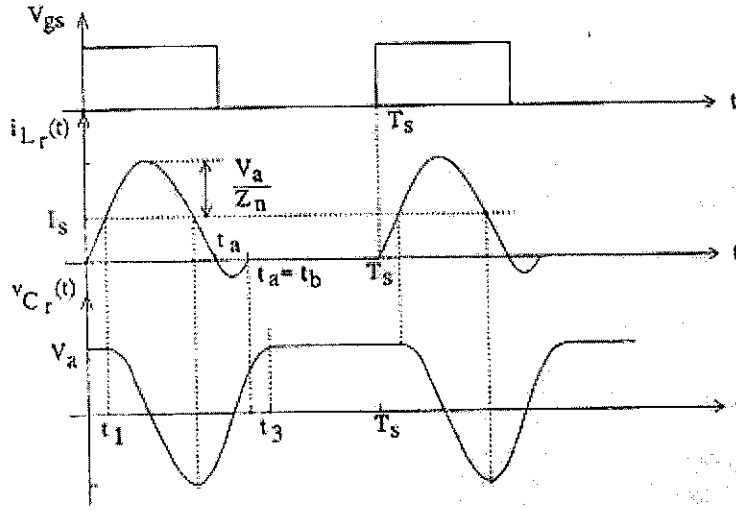
Figure 16: Waveforms of full-wave ZCS quasi-resonant boost converter [14]

Mode 3 ($t_2 < t \le t_3$):

Mode 3 begins after the resonant inductor current decreases to zero from its negative peak at time t_2. The switching transistor, Q_s, switches off and its drain-to-source voltage continues to rise during this interval. The equivalent circuit is shown in **Figure 17**. The resonant capacitor continues to charge toward the output voltage, V_a, by the input current, I_s. The rate of increase of the capacitor voltage is:

$$\frac{dv_{C_r}(t)}{dt} = \frac{I_s}{C_r}$$

20

The initial resonant capacitor voltage is:

$$v_{Cr}(t_2) = V_a \cos \alpha$$

The duration of mode 3, T_3, is:

$$T_3 = \frac{C_r V_a (1 - \cos \alpha)}{I_s}$$
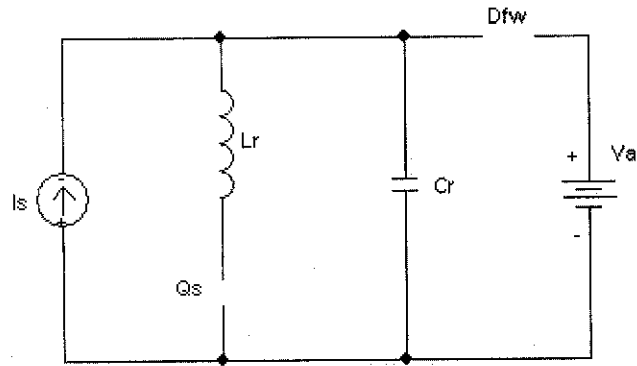
Figure 17: Mode 3 equivalent circuit of the ZCS quasi-resonant boost converter

Mode 4 ($t_3 < t \le t_4$):

Mode 4 begins when the resonant capacitor voltage reaches V_a at t_3. The freewheeling diode, D_{fw}, is forward biased and switched on. The equivalent circuit is shown in **Figure 18**.
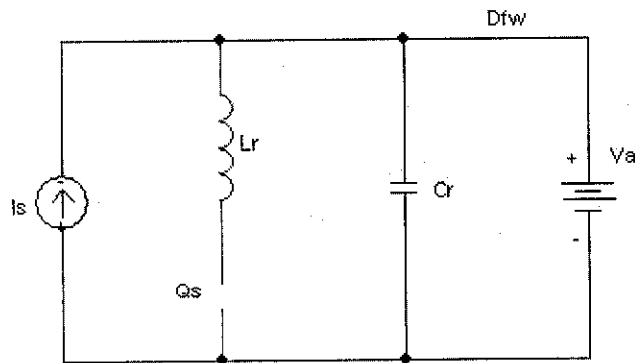
Figure 18: Mode 4 equivalent circuit of the ZCS quasi-resonant boost converter

The duration of mode 4 is:

$$T_4 = T_s - T_1 - T_2 - T_3, \text{ where } T_s \text{ is the switching period}$$

The voltage conversion ratio of the full-wave ZCS quasi-resonant boost converter can be found by imposing the constant volt-second relationship on the input inductor, L_i, since the average voltage across it is zero for steady-state operation. The average voltage across the input inductor during the time interval between t_1 and t_3 (i.e., the resonant period T_n) is V_s since the average V_{Cr} is zero. During the remaining time interval (i.e., $T_s - T_n$), the average voltage across the input inductor is $V_s - V_a$. Thus,

$$V_s T_n + (T_s - T_n)(V_s - V_a) = 0$$

The voltage conversion ratio for the full-wave ZCS quasi-resonant boost converter is:

$$\frac{V_a}{V_s} = \frac{1}{1 - f_s / f_n}$$

This voltage conversion ratio is similar to that of the conventional boost switching converter if the ratio of the switching frequency to the resonant frequency is replaced by its duty cycle, D. The voltage conversion ratio versus f_s/f_n relationship for a full-wave ZCS quasi-resonant boost converter is shown in **Figure 19**. It should be noted that the switching frequency, f_s, must be smaller than the resonant frequency. In a half-wave ZCS quasi-resonant boost converter, the output voltage is very sensitive to load variations. Thus the only means to regulate its output voltage is to change the switching frequency. On the other hand, the full-wave ZCS quasi-resonant boost converter is able to regulate its output voltage against load variation without a large change in switching frequency.
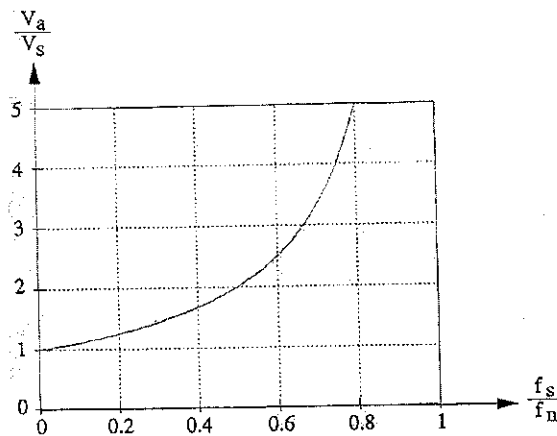
Figure 19: Voltage conversion ratio versus f_s/f_n of a full-wave ZVS quasi-resonant boost converter [14]

Figure 20 shows the circuit schematic of a full-wave zero-current-switching (ZVS) quasi-resonant boost converter.
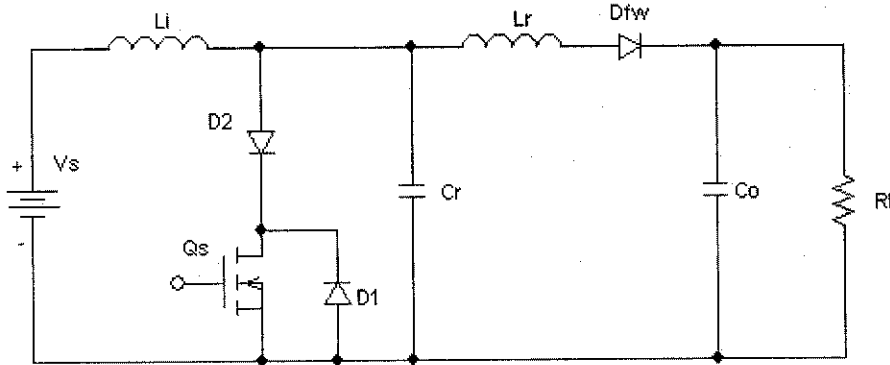
Figure 20: Circuit schematic a full-wave ZVS quasi-resonant boost converter

The operation of the ZCS quasi-resonant boost converter can also be divided into four modes. Suppose before the switching transistor, Q_s, is switched off, it carries the input current, I_s. Also, the freewheeling diode, D_{fw}, is switched off [15].

Mode 1 *($0 < t \le t_1$)*:

Mode 1 begins when the switching transistor, Q_s, is switched off at $t = 0$. The resonant capacitor, C_r, is charged up and its voltage increases according to:

$$C_r \frac{dv_{Cr}}{dt} = I_s$$

The duration of mode 1, T_1, is:

$$T_1 = C_r \frac{V_o}{I_s}$$

Thus, mode 1 is characterized by the charging of the resonant capacitor and the storage of energy in electrostatic form. Both the switching transistor and the freewheeling diode are switched off during mode 1 as shown by the equivalent circuit shown in **Figure 21**
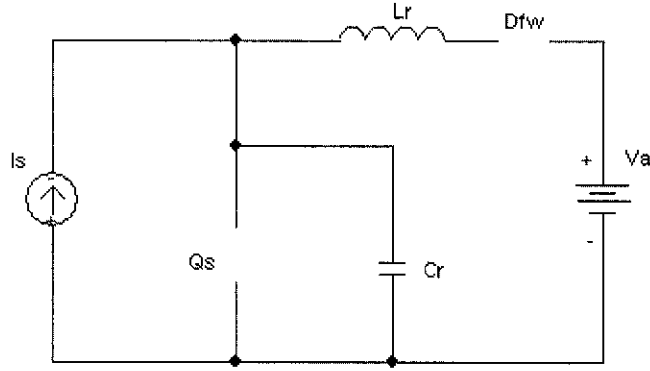
Figure 21: Mode 1 equivalent circuit of the ZVS quasi-resonant boost converter

Mode 2 $(t_1 < t \le t_2)$:

Mode 2 begins when the voltage across the resonant capacitor reaches the steady-state output voltage; V_a. Diode D_{fw} is forward biased and switched on. Current starts to flow through the resonant inductor. The equivalent circuit is shown in **Figure 22**.
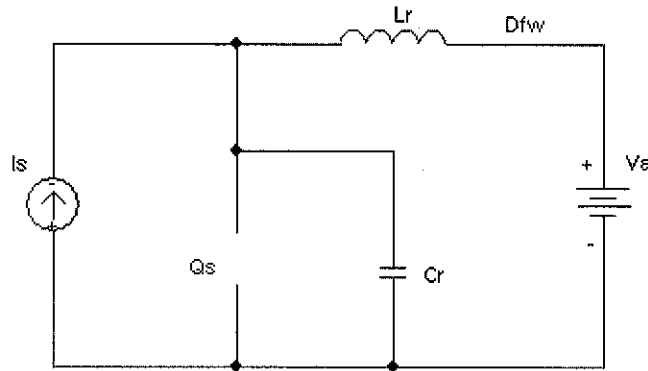
Figure 22: Mode 2 equivalent circuit of the ZVS quasi-resonant boost converter

The rate of increase of the resonant inductor current, $i_{Lr}(t)$, is:

$$\frac{di_{Lr}(t)}{dt} = \frac{v_{Cr}(t) - V_a}{L_r}$$

The voltage across the resonant capacitor continues to increase beyond the steady-state output voltage, V_a, according to:

$$C_r \frac{dv_{Cr}}{dt} = I_s - i_{Lr}(t)$$

The expressions for $i_{Lr}(t)$ and $v_{Cr}(t)$ can be found by using the initial conditions $i_{Lr}(t_1)=0$ and $v_{Cr}(t_1) = V_a$. The resonant inductor current, $i_{Lr}(t)$, and the resonant capacitor voltage, $v_{Cr}(t)$, are:

$$i_{Lr}(t) = I_s(1 - \cos\omega_n t)$$

$$v_{Cr}(t) = V_a + I_s Z_n \sin\omega_n t$$

Where, $Z_n = \sqrt{L_r / C_r}$ is the circuit characteristic impedance and $\omega_n = 1/\sqrt{L_r C_r}$ is the resonant frequency.

Mode 2 is known as resonant mode. The resonant capacitor voltage continues to swing to the negative cycle as it feeds energy back to the input source as shown in **Figure 23**. The duration of the resonant mode, $T_2 = t_2 - t_1$, can be found by setting $v_{Cr}(T_2) = 0$. The duration of this resonant mode, $T_2 = t_2 - t_1$, can be found by setting $v_{Cr}(T_2) = 0$:

$$v_{Cr}(T_2) = V_a + I_s Z_n \sin\omega_n t$$

The duration for mode 2, T_2, is:

$$T_2 = \frac{\sin^{-1}(-V_a / I_s Z_n)}{\omega_n} = \frac{\alpha}{\omega_n}$$

(α takes on values between 1.5π and 2π)

The resonant mode terminates after all the stored energy in the resonant capacitor has been fed back to the input source. The switching transistor, Q_s, should be switched on during the negative resonant capacitor voltage cycle. Otherwise, the resonant capacitor will begin to recharge and the switching transistor will miss the opportunity to switch on at the zero-voltage condition. The input current, I_s, must be smaller than V_a/Z_n for the switching transistor to switch off during zero current [16].
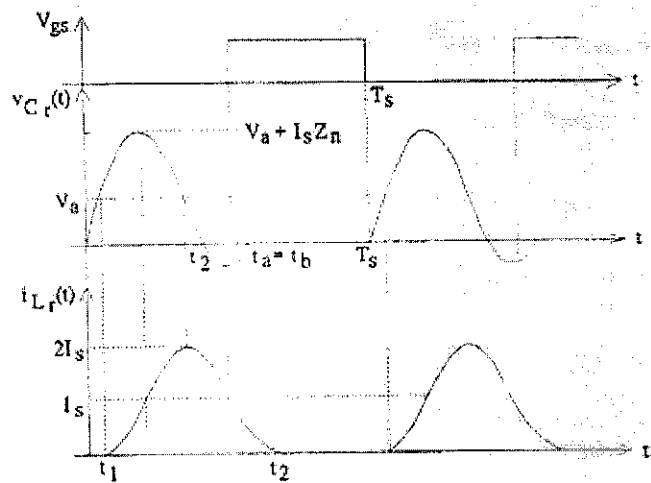
Figure 23: Waveforms of full-wave ZVS quasi-resonant boost converter [17]

Mode 3 ($t_2 < t \le t_3$):

Mode 3 begins after the resonant capacitor voltage decreases to zero from its negative peak at time t_2. **Figure 24** shows the equivalent circuit. Both Q_s and D_{fw} are switched on during this mode. The resonant inductor current continues to decrease according to:

$$L_r \frac{di_{Lr}}{dt} = -V_a$$

The initial resonant inductor current is:

$$i_{Lr}(t_2) = I_s(1 - \cos\alpha)$$

The duration of mode 3, T_3, is:

$$T_3 = \frac{L_r I_s(1 - \cos\alpha)}{V_a}$$
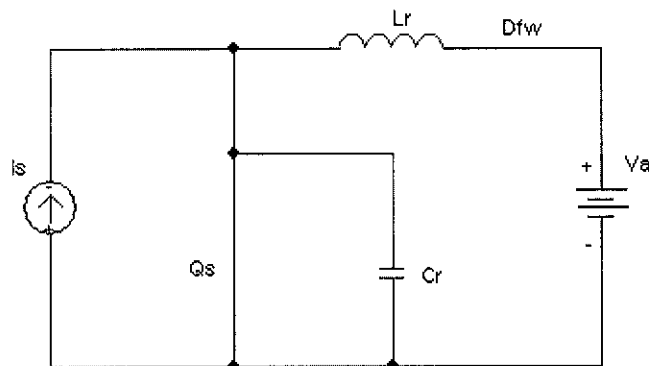
Figure 24: Mode 3 equivalent circuit of the ZVS quasi-resonant boost converter

26

Mode 4 ($t_3 < t \le t_4$):

Mode 4 begins when the resonant inductor current decrease to zero at t_3. The freewheeling diode, D_{fw}, is now reverse biased and switched off at time t_3. The equivalent circuit is shown in **Figure 25**.
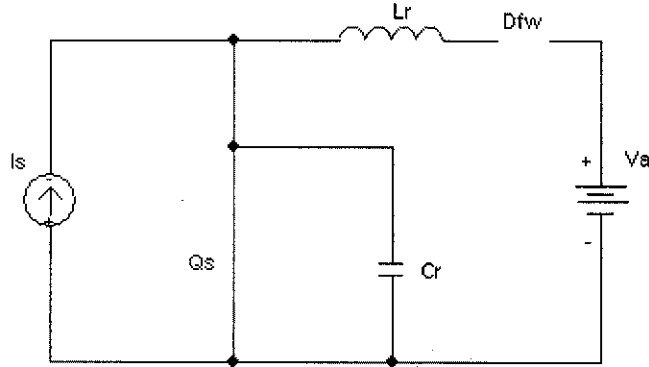
Figure 25: Mode 4 equivalent circuit of the ZVS quasi-resonant boost converter

The duration of mode 4 is:

$$T_4 = T_s - T_1 - T_2 - T_3, \text{ where } T_s \text{ is the switching period}$$

The voltage conversion ratio of the full-wave ZVS quasi-resonant boost converter can be found by imposing the constant volt-second relationship on the input inductor, L_i, since the average voltage across it is zero for steady-state operation. The average voltage across the input inductor during the time interval between t_1 and t_3 (i.e., the resonant period T_n) is $V_s - V_a$. During the remaining time interval (i.e., $T_s - T_n$), the average voltage across the input inductor is V_s. Thus,

$$(V_s - V_a)T_n + (T_s - T_n)V_s = 0$$

The voltage conversion ratio for the full-wave ZCS quasi-resonant boost converter is:

$$\frac{V_a}{V_s} = \frac{f_n}{f_s}$$

The voltage conversion ratio versus f_s/f_n relationship for a full-wave ZVS quasi-resonant boost converter is shown in **Figure 26**. As shown, the voltage conversion ratio is inversely proportional to the f_s/f_n ratio. It should be noted that the switching frequency, f_s, must be smaller than the resonant frequency. In a half-wave ZCS quasi-resonant boost converter, the output voltage is very sensitive to load variations. Thus the only means to regulate its output voltage is to change the switching frequency. On the other hand, the

27

full-wave ZCS quasi-resonant boost converter is able to regulate its output voltage against load variation without a large change in switching frequency [18].
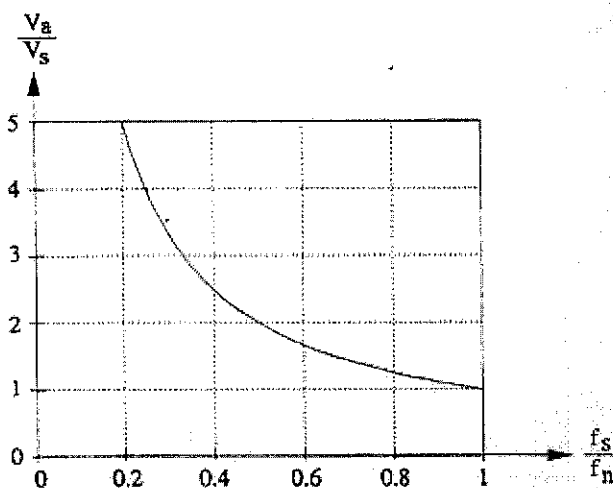
Figure 26: Voltage conversion ratio versus f_s/f_n of a full-wave ZVS quasi-resonant boost converter [19]

2.1.5 Snubber Circuits

In general, snubber circuits in converter design are effective in reducing the voltage and current stress encountered by switches and diodes experienced in PWM design. Snubber circuit also reduces ringing and oscillation during switching. In other words, snubber circuits can control the EMI radiation. They also improve efficiency but have the disadvantage of slightly higher cost of devices. There are three different types of snubber circuits:

1. Active snubbers (non-dissipative): this type requires capacitor (C), inductor (L), diode (D) and an extra switch to control the voltage and current waveforms while energy captured is recycled back to the power source or to the load.

2. Passive dissipative snubber: this type uses resistor (R), diode (D), capacitor (C) or inductor (L) to control the voltage and current while energy captured is dissipated in the resistor.

3. Passive lossless snubber: this type requires capacitor (C), inductor (L) and diode (D) to control the voltage and current waveforms while energy captured is recycled back to the power source or the load.

To achieve ZCS condition, the snubber inductor is usually placed in the circuit to control the *di/dt*. The snubber diode discharges the store-energy of the snubber inductor. The capacitor discharging process is normally arranged to occur over the semiconductor switch to achieve the ZVS condition [20].

In this project, an active snubber circuit consisting of a clamp capacitor in series with an auxiliary switch and a snubber inductor is employed. The snubber inductor controls the *di/dt* rate of the boost rectifier during its turn-off. The energy from the snubber inductor after the main switch turn-off is returned to the input or delivered to the output via the active snubber. The active snubber circuit used in the project is shown below:
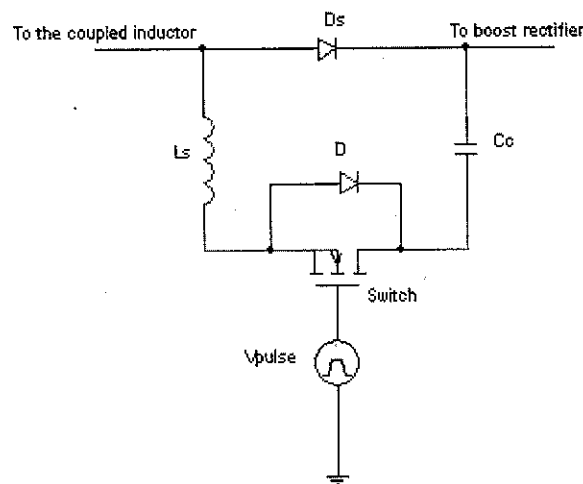
Figure 27: The proposed active snubber circuit

In addition, a clamp diode is connected between the ground and the anode of the snubber diode D_s, which is in series with boost rectifier in order to eliminate the parasitic ringing between the junction capacitance of the boost rectifier and the snubber inductor, the stress of the boost rectifier is minimized. Figure below shown the combination of the snubber circuit and clamp capacitor

29
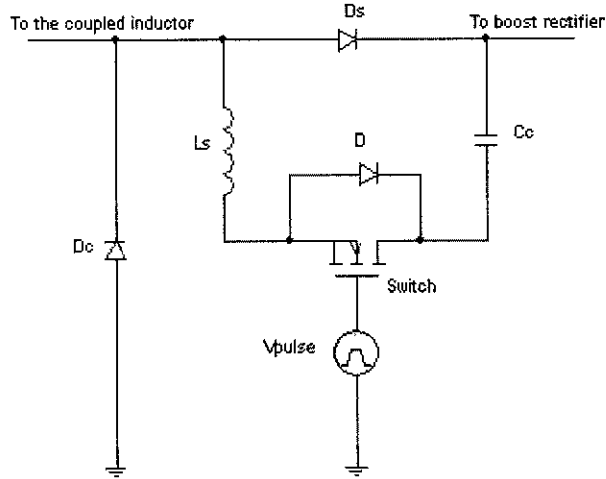
Figure 28: Combination of the active snubber circuit and a clamp capacitor.

The combination of the active snubber circuit and a clamp capacitor is added into the original soft-switched quasi-resonant DC/DC boost converter in order to improve the efficiency, reduce the voltage stress on the main switch and the boost rectifier, and thus improve the EMI radiation performance of the original circuit.

2.2 Modified Circuit Operation

To simplify the analysis of operation, it is assumed that the inductance of boost inductor L_{r1} is large so that it can be represented by constant-current source I_{in}, and the output-ripple voltage is negligible so that the voltage across the output filter capacitor can be represented by constant-voltage source V_o. The circuit diagram of the simplified converter is shown in **Figure 29.** In addition, it is assumed that in the on-state, semiconductors exhibit zero resistance, i.e., they are short circuits. However, the output capacitances of the MOSFETs and the reverse-recovery charge of the rectifier are not neglected in this analysis. To further facilitate the explanation of operation, **Figure 30** to **Figure 37** shows topological stages of the circuit during a switching cycle. It should be noted that because the junction capacitance of boost rectifier D_s has been neglected for the time being and the clamp diode D_c is not shown in **Figure 30** to **Figure 37** since it never conducts.
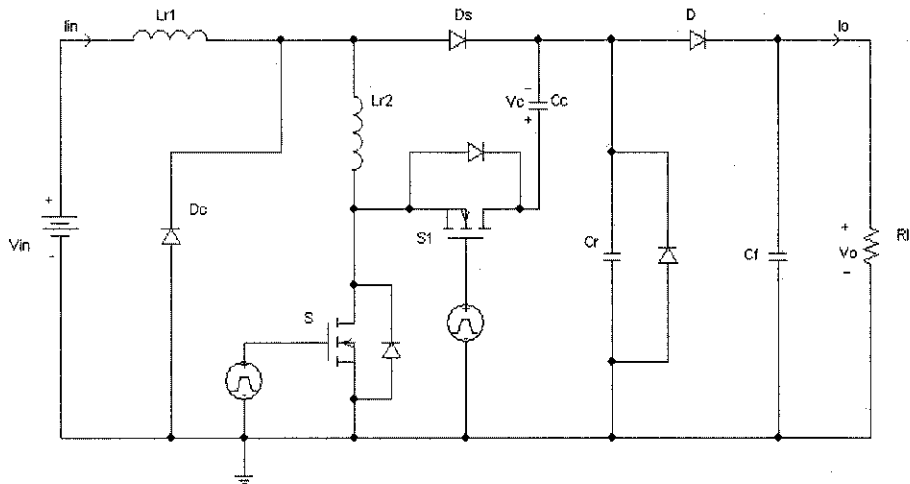
Figure 29: Modified soft-switched quasi-resonant DC/DC boost converter with an active snubber circuit and a clamp capacitor.

The operation of the modified soft-switched quasi-resonant converter can be divided into 8 modes.

Mode 1:
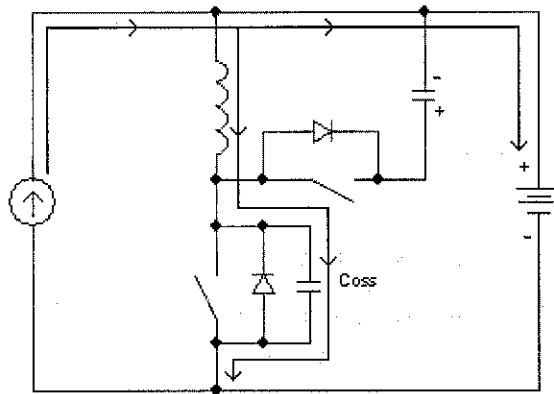
Figure 30: Mode 1 *[T₀, T₁]*

Mode 1 begins at $t = T_o$, when the main switch S is turned off. The entire input current I_{in} flows through inductor L_{r2} and switch S. At the same time, rectifier D_s is off with a reverse voltage across its terminals equal to output voltage V_o. Auxiliary switch S_1 is also

31

off, blocking the voltage $V_o + V_c$, where V_c is the voltage across the clamp capacitor and V_o is the output voltage.

After the switch S is turned off at $t = T_o$, the current which was flowing through the channel of the MOSFET is delivered to the output capacitance of the switch, C_{oss}, as shown in **Figure 30**. As a result, the voltage across switch S starts linearly increasing due to the constant charging current I_{in}. During this stage, auxiliary switch voltage v_{s1} decreases from $V_o + V_c$ towards zero, while main switch voltage v_s increase from zero towards $V_o + V_c$. When voltage across switch S reaches V_o, snubber diode D_s starts conducting, and the current through inductor L_{r2} starts decreasing due to a negative voltage across its terminal. This topological stage ends at $t = T_1$, when voltage v_s reaches $V_o + V_c$ and the antiparallel diode of switch S_1 starts conducting. At that moment, the remaining inductor current i_{Lr1} is diverted into clamp capacitor C_c, and switch voltage v_s is clamped to $V_o + V_c$, as shown in **Figure 31**.

Mode 2:
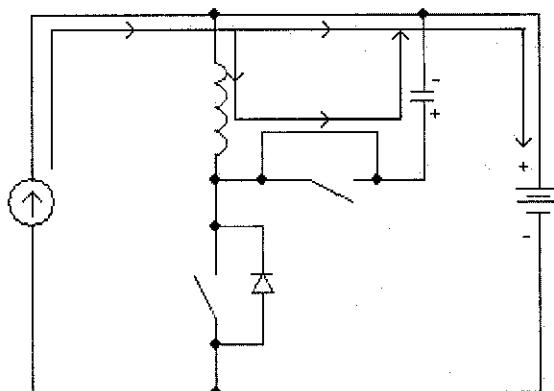
Figure 31: Mode 2 *[T₁, T₃]*

Mode 2 begins at $t = T_1$. During mode 2 inductor current i_{Lr1} continues to decrease as it discharges to clamp capacitor C_c. If the capacitance of the C_c is large, capacitor voltage v_c is almost constant and inductor current i_{Lr1} decrease linearly. Otherwise, i_{Lr1} decrease in a resonant fashion. As i_{Lr1} decreases, snubber diode current i_{Ds} increases at the same rate because the sum of $i_{Lr1} + i_{Ds}$ is equal to constant input current I_{in}. This topological stage ends at $t = T_3$, when i_{Lr1} reaches zero and the antiparallel diode of auxiliary switch S_1 stops conducting. To achieve ZVS of S_1, it is necessary to turn on the transistor of switch

32

S1 before $t = T_3$, i.e., while its antiparallel diode is conducting. The MOSFET of switch S_1 is turned on at $t = T_2$ (T_2 is in between $[T_1, T_3]$).
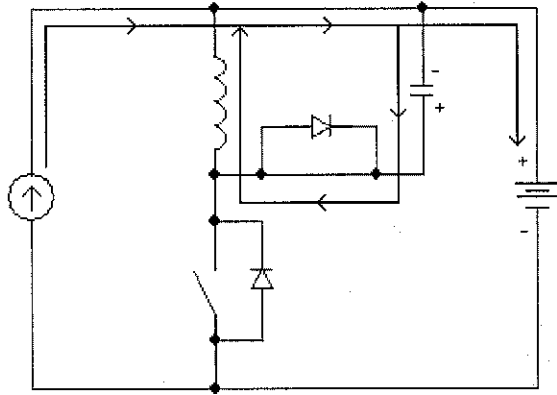
Mode 3:

Figure 32: Mode 3 *[T₃, T₄]*

Mode 3 begins at $t = T_3$. The transistor of switch S_1 is turned on prior to $t = T_3$, inductor current i_{Lr1} will continue to flow after $t = T_3$ in the opposite direction through the closed transistor, as shown in **Figure 32**. At the same time, snubber diode current i_{Ds} will continue to increase at the same rate, exceeding the input-current level I_{in}. During the topological stage, the energy stored in clamp capacitor C_c during interval $[T_1, T_3]$ is returned to the inductor in the opposite direction. This interval ends at $t = T_4$ when auxiliary switch is turned off.
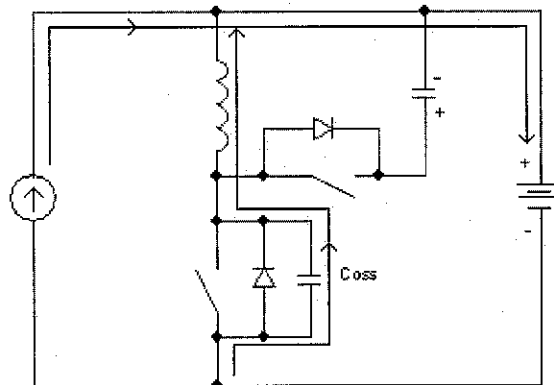
Mode 4:

Figure 33: Mode 4 *[T₄, T₅]*

Mode 4 starts at $t = T_4$ when the switch S_1 is turned off, conductor current i_{Lr1} can not flow anymore through clamp capacitor C_c. Instead, it continues to flow through output capacitance C_{oss} of the switch S, as shown in **Figure 33**. Since i_{Lr1} discharges C_{oss}, main switch voltage v_s decrease from $V_o + V_c$ towards zero. At the same time, i_{Lr1} increases towards zero and i_{Ds} decreases toward I_{in}.

Whether v_s will decrease all the way to zero depends on the energy stored in inductor L_{r1} at $t = T_4$. If this energy is larger than the energy required to discharge C_{oss} from $V_o + V_c$ down to zero, i.e., if

$$(1/2) \; L_{r1} \; [\; i_{Lr1}(t = T_1)]^2 \geq (1/2) \; C_{oss} \; (V_o + V_c)^2$$

Then v_s will reach zero. Otherwise, v_s will not be able to fall to zero, and will tend to oscillate around the V_{in} level if main switch S is not turned on immediately after v_s reaches its minimum. Assuming that inductor energy is more than enough to discharge C_{oss} to zero, v_s will reach zero at $t = T_5$, while inductor current i_{Lr1} is still negative. Mode 4 ends at $t = T_5$.

Mode 5:
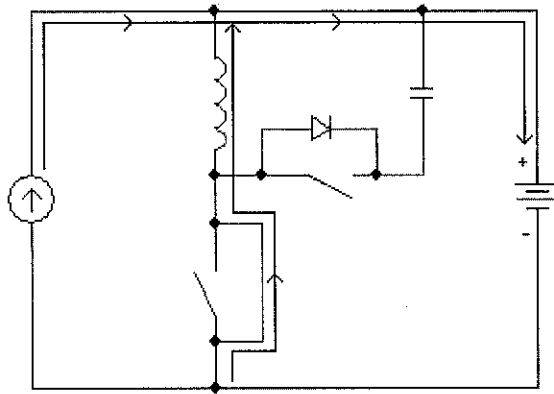
Figure 34: Mode 5 *[T_5, T_6]*

Mode 5 starts at $t = T_5$, when v_s reaches zero while inductor current i_{Lr1} is still negative. As a result, the antiparallel diode of S will start conducting as shown in **Figure 34**. Because of the simultaneous conduction of he antiparallel diode of S and snubber diode D_s, constant output voltage V_o is applied to inductor L_{r2} so that inductor current i_{Lr1} increase linearly towards zero. To achieve ZVS of switch S, it is necessary to turn on the

34

transistor of switch S during interval $[T_5, T_6]$ when the antiparallel diode of S id turned on during this interval, i_{Lrl} will continue to increase linearly after $t = T_6$, as shown in **Figure 35.**

Mode 6:
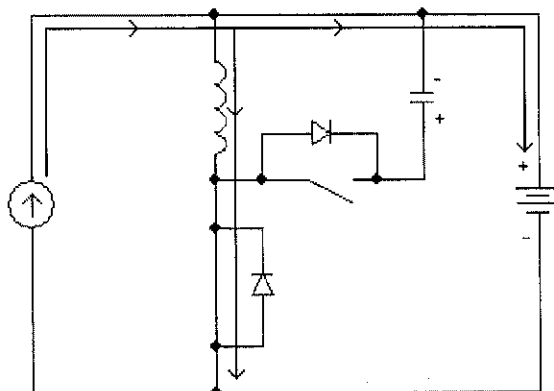
Figure 35: Mode 6 $[T_6, T_7]$

Mode 6 begins at $t = T_6$. After this time, the inductor current i_{Lrl} continues to increase linearly from the previous stage. At the same time, snubber diode i_{Ds} will continue to decrease linearly. The rate of i_{Ds} decrease is determined by the value of L_{r2} inductance because:

$$\frac{di_{Ds}}{dt} = -\frac{V_o}{L_{r2}}$$

To reduce the rectifier-recovery charge and the associated losses, a proper inductance needs to be selected. Generally, a larger inductance, which gives a lower di_{Ds}/dt rate, results in a more efficient reduction of the reverse-recovery-associated losses. The mode ends at $t = T_7$, when i_{Lrl} reaches the input-current level I_{in}, and the snubber diode current i_{Ds} falls to zero.
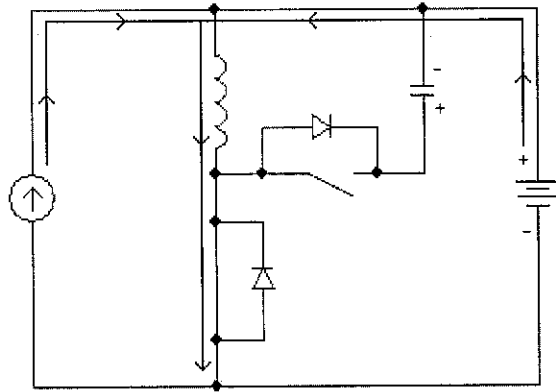
Mode 7:

Figure 36: Mode 7 *[T$_7$, T$_8$]*

Mode 7 begins at $t = T_7$, when the inductor current i_{Lr1} increases linearly to the input-current level I_{in}, and the snubber diode current i_{Ds} falls to zero. However, due to the residual stored charge, snubber diode current i_{Ds} starts flowing in the reverse direction, as shown in **Figure 36**, producing an overshot of the switch current over the I_{in} level. Without L_{r2} this reverse-recovery current would be many times larger. This mode ends at $t = T_8$ when the junction capacitance of the snubber diode affects the circuit operation after the snubber diode D_s has recovered at $t = T_8$.
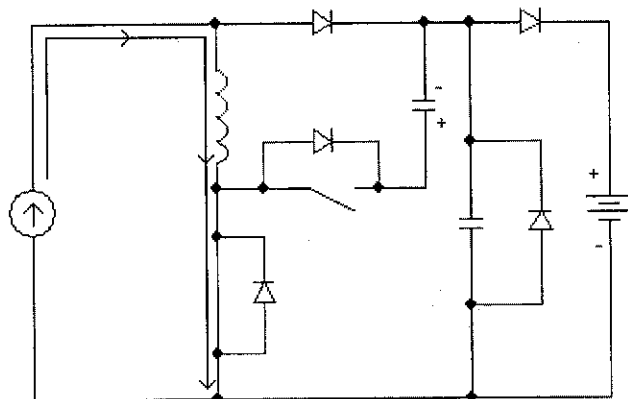
Mode 8:

Figure 37: Mode 8 *[T$_8$, T$_9$]*

Mode 8 begins at $t = T_8$, when the junction capacitance of the snubber diode D_s affects the circuit operation after snubber diode has recovered. Once the snubber diode has

recovered, the entire input current I_{in} flows through switch S until the next switching cycle is initiated at $t = T_9$, as shown in **Figure 37**.

CHAPTER 3

METHODOLOGY AND PROJECT WORK

3.1 Procedure

Figure 38 below describes the methodology of the project:

```
        ┌─────────────────────────┐
        │       Research          │
        │   Soft-switched quasi-  │
        │   resonant DC/DC boost  │
        │       converter         │
        └─────────────────────────┘
                    │
                    ▼
        ┌─────────────────────────┐
        │  Design and Simulation  │◄────────────┐
        │  Design circuit, Determine│            │
        │     circuit parameters  │             │
        │    Simulation in PSPICE │             │
        └─────────────────────────┘             │
                    │                           │
                    ▼                           │
        ┌─────────────────────────┐             │
        │  Performance Analysis   │             │
        │    Power efficiency &   │             │
        │    Switch performance   │             │
        └─────────────────────────┘             │
                    │                           │
                    ▼                           │
               ╱─────────╲                      │
              ╱    Meet    ╲─────────────────────┘
              ╲ Expectations?╱
               ╲─────────╱
                    │
                    ▼
        ┌─────────────────────────┐
        │    Technical Report     │
        │                         │
        └─────────────────────────┘
```
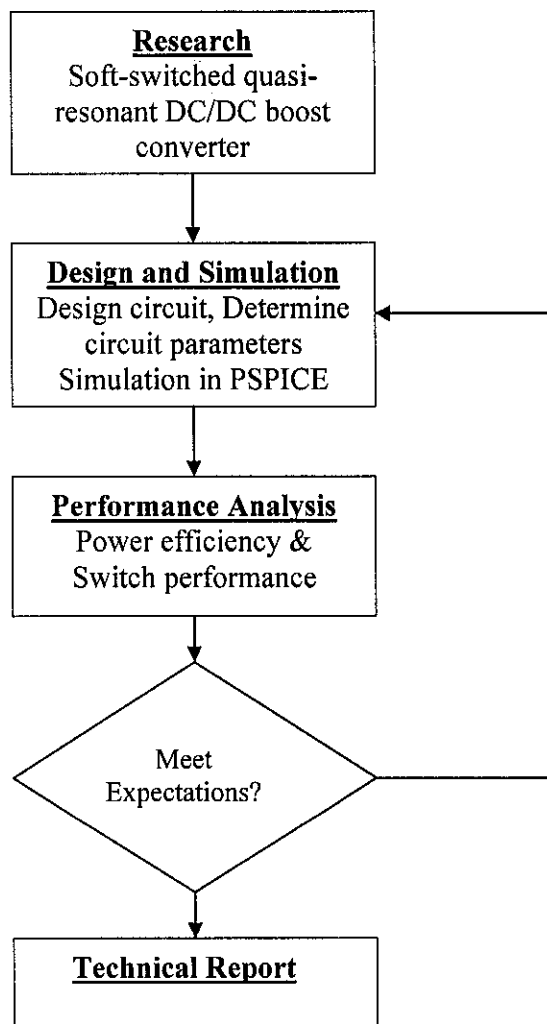
Figure 38: Flow chart of the methodology of the project

3.1.1 Research

Prior to the design of a novel soft-switched quasi-resonant DC/DC boost converter, researches have been done on the most recent studies of soft-switched quasi-resonant DC/DC boost converter. Study on combined snubber networks also has been done to understand the functionality. Further researches have been carried out on switching loss in switch, leakage spike in current and voltage and all the application waveforms.

3.1.2 Simulation in PSPICE

First of all, simulation on the most recent study of the soft-switched quasi-resonant DC/DC boost converter in Ba-Thunya and Prasad's study has been done. Figure shows the original circuit in their study:

Original soft-switched quasi-resonant DC/DC boost converter
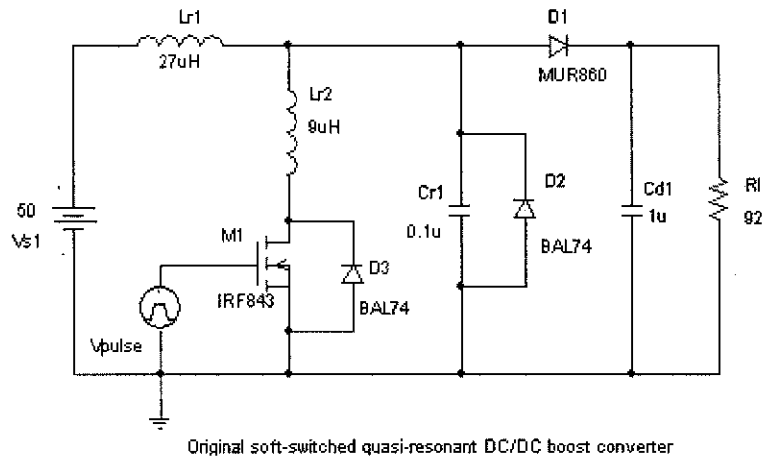
Figure 39: The original soft-switched quasi-resonant DC/DC boost converter in Ba-Thunya and Prasad's study

The basic settings used in Ba-Thunya and Prasad's study:

1. Frequency, f_s = 167 kHz , T = 6 μs
2. Output voltage, V_o = 60V
3. Duty ratio, D = 1/6
4. Output power, P_o = 40 W

Components used in Ba-Thunya and Prasad's study:

1. Switch (V_{pulse}) – Power MOSFET (N-channel) type: IRF843

Absolute Maximum Ratings:

Parameter	Symbol	IRF843
Drain-Source Voltage	V_{ds}	450 V
Drain-Gate Voltage (R_{gs}=1mΩ)	V_{dg}	450 V
Gate-Source Voltage	V_{gs}	±20 V
Operating frequency	f_s	250 KHz
Drain Current Continuous Pulse	I_d	7 A
	I_{dM}	28 A
Total Power Dissipation at T_c = 25°C	P_D	125 W

Table 1: Absolute maximum ratings of Power MOSFET (N-channel) IRF843

Settings:

i. Period , PER = 6 μs

ii. Pulse Width, PW = 1 μs

iii. Delay time, T_D = 0

iv. Fall time, T_F = 0

v. Rise time, T_R = 0

vi. V_1 = 0V

vii. V_2 = 5V

2. Boost rectifier D_1, type MUR860

Absolute Maximum Ratings:

Parameter	Symbol	MUR860
Peak Repetitive Reverse Voltage	V_{RRM}	600 V
Working Peak Reverse Voltage	V_{RWM}	600 V
DC Blocking Voltage	V_R	600 V
Operating frequency	f_s	250 KHz
Average Rectified Forward Current Total Device, (Rated V_R, Square Wave, 20 kHz), T_C = 150 °C	$I_{F(AV)}$	8 A
Peak Repetitive Forward Current (Rated V_R, Square Wave, 20 kHz), T_C = 150 °C	I_{FM}	16 A
Non-repetitive Peak Surge Current	I_{FSM}	100A

Table 2: Absolute maximum ratings of Power Rectifier MUR860

3. Power diodes D_2, D_3, type BAL74

Absolute Maximum Ratings:

Parameter	Symbol	BAL74
Continuous Reverse Voltage	V_R	50 V
Operating frequency	f_s	250 KHz
Average Output Rectified Current (t_{av} = 10ms)	I_o	100 mA
Continuous Forward Current	I_F	150 mA
Peak Forward Current (t = 15ms)	I_{FM}	200 mA
Forward Surge Current (t = 1μs)	I_{FS}	1 A
Operating and Storage Temperature Range	T_j, T_{stg}	-55 to 150 °C
Power Dissipation at T_{amb} = 25 °C	P_{tot}	330 mW

Table 3: Absolute maximum ratings of High-Switching Power Diode BAL74

4. Coupled inductors L_{r1}, L_{r2}

    i. L_{r1} = 27 μH

    ii. L_{r1} = 9 μH

5. Load Resistance (R_l)

    i. R_l = 92 Ω

6. Capacitance (C_{r1}, C_{d1})

    i. C_{r1} = 0.047 μF

    ii. C_{d1} = 0.1 μF

7. DC power supply (V_{s1})

    i. V_{s1} = 50 V

After understanding the concept of snubber network using an auxiliary switch, the design of the modified soft-switched quasi-resonant DC/DC boost converter with a snubber circuit and a clamping diode has been done. Figure show the proposed circuit. Then, the performance of the proposed circuit will be evaluated in PSPICE simulation in order to meet the project's objectives.

The parameter of clamped capacitor in the snubber circuit has been calculated by using following equations:

$$\omega_n C_c = \frac{1}{\omega_n L_{r4}}$$

$$\omega_n = \frac{1}{\sqrt{L_{r4} C_c}}$$

$$C_c = \frac{1}{\omega_n^{2} L_{r4}} = \frac{1}{(2\pi f_s)^2 L_{r4}} = \frac{1}{(2\pi 167k)^2 9\mu} = 0.1\mu F$$
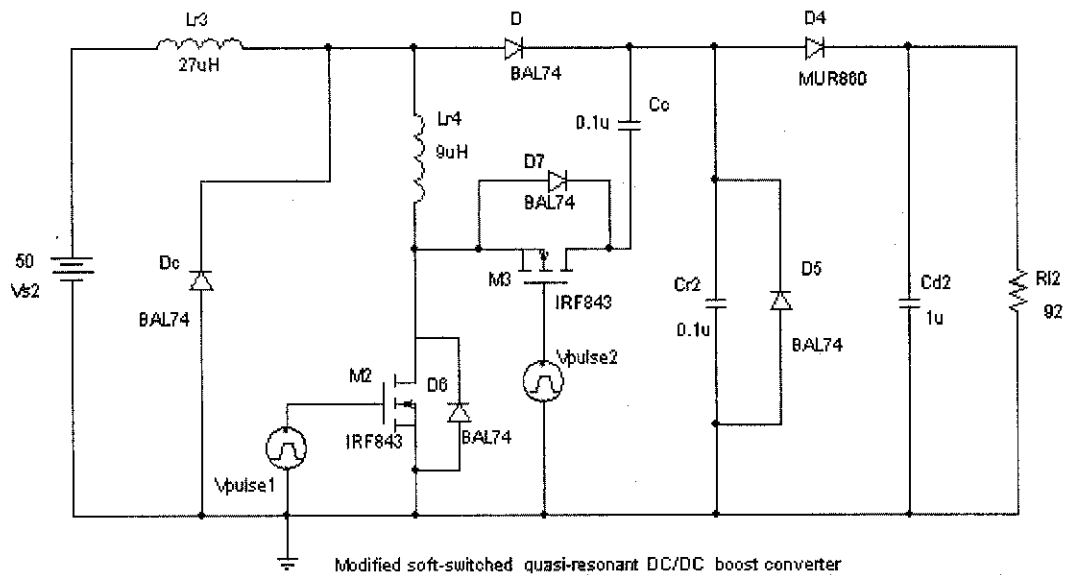
Figure 40: The modified soft-switched quasi-resonant DC/DC boost converter with a snubber circuit and a clamping diode

The basic settings are maintained from Ba-Thunya and Prasad's study:

1. Frequency, f_s = 167 kHz, T = 6 µs
2. Output voltage, V_o = 60V
3. Duty ratio, D = 1/6
4. Output power, P_o = 40 W

Components in the proposed circuit:

1. Main Switch (V_{pulse1}) – Power MOSFET (N-channel) type: IRF843
    i. Period , $PER = 6$ μs
    ii. Pulse Width, $PW = 1$ μs
    iii. Delay time, $T_D = 0$
    iv. Fall time, $T_F = 0$
    v. Rise time, $T_R = 0$
    vi. $V_1 = 0$V
    vii. $V_2 = 5$V

2. Auxiliary Switch (V_{pulse2}) – Power MOSFET (N-channel) type: IRF843
    i. Period , $PER = 6$ μs
    ii. Pulse Width, $PW = 4.5$ μs
    iii. Delay time, $T_D = 1.3$ μs
    iv. Fall time, $T_F = 0$
    v. Rise time, $T_R = 0$
    vi. $V_1 = 0$V
    vii. $V_2 = 5$V

3. Boost rectifier D_4 type MUR860

4. Power diodes D, D_c, D_5, D_6, D_7 type BAL74

5. Coupled inductors L_{r3}, L_{r4}
    i. $L_{r3} = 27$ μH
    ii. $L_{r4} = 9$ μH

6. Load Resistance (R_{l2})
    i. $R_{l2} = 92$ Ω

7. Capacitance (C_{r2}, C_{d2}, C_c)
    i. $C_{r2} = 0.047$ μF
    ii. $C_{d2} = 0.1$ μF
    iii. $C_c = 6$ μF

8. DC power supply (V_{s2})
    i. $V_{s2} = 50$ V

CHAPTER 4

RESULTS AND DISCUSSION

4.1 Result Analysis

Figure 41 below shows the schematic diagrams of the soft-switching quasi-resonant DC/DC boost converter and the modified soft switching quasi-resonant DC/DC boost converter with an active snubber circuit.
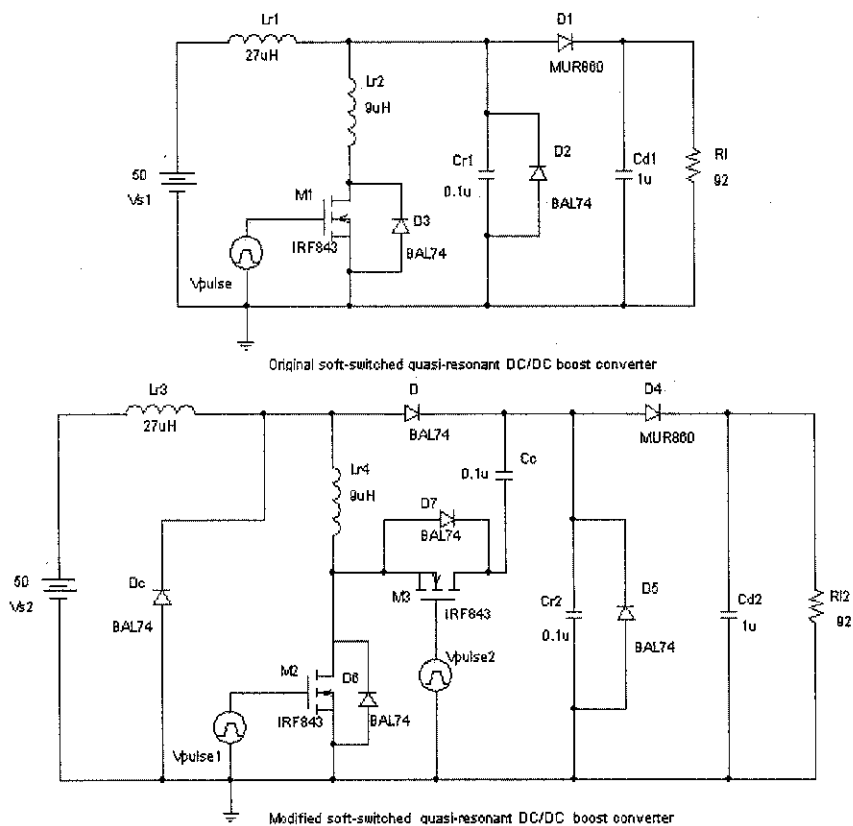
Figure 41: Schematic diagrams of the original converter and the modified converter

44

The circuit (shown in **Figure 41**) uses n-type MOSFET auxiliary switch M_3 and clamp capacitor C_c connected in series to discharge the energy stored in the snubber inductor L_{r4} to the output after M_3 is turned off. Diode D_c is employed to eliminate the parasitic ringing between the junction capacitance of D and inductor L_{r4} by clamping the anode of D to ground. Following are the improvements shown in PSPICE simulation:

4.1.1 Output ripple voltage

Figure 42 below shows the output waveforms of the original boost converter and the modified boost converter with an active snubber.
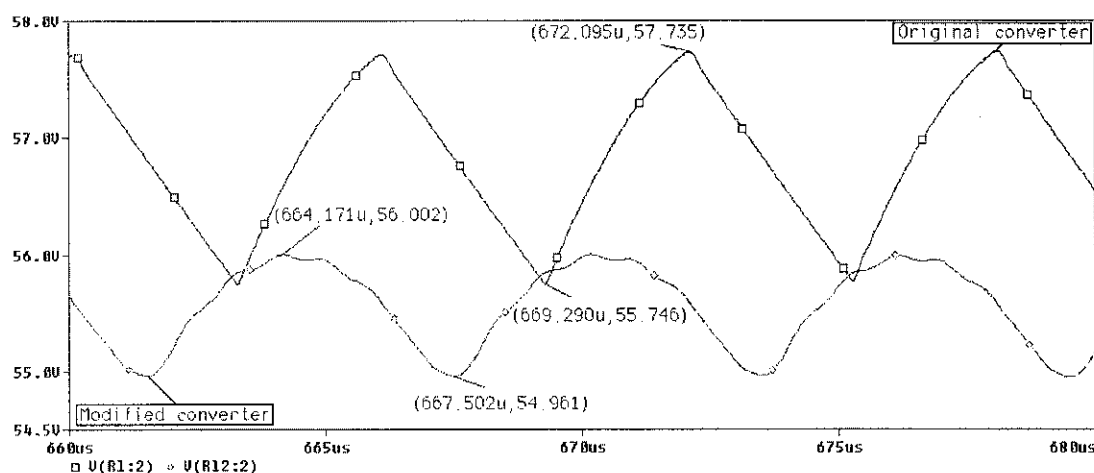
Figure 42: Output ripple voltage of the original boost converter [V(R1:2)] and the modified boost converter with an active snubber [V(R12:2)]

The output ripple voltage of the original boost converter:

$$V_{out1(ripple)} = \frac{57.735 - 55.746}{(57.735 + 55.746)/2} = 3.51\%$$

The output ripple voltage of the modified boost converter with an active snubber:

$$V_{out2(ripple)} = \frac{56.002 - 54.961}{(56.002 + 54.961)/2} = 1.88\%$$

The modified boost converter with an active snubber introduces an improvement in the output ripple voltage (decrease from 3.51 % to 1.88 %), improvement of 46.4 %. Hence, the DC output characteristic of the converter has been improved.

4.1.2 Power Efficiency

Figure 43 below shows the waveforms of input power of the original boost converter and the modified boost converter.
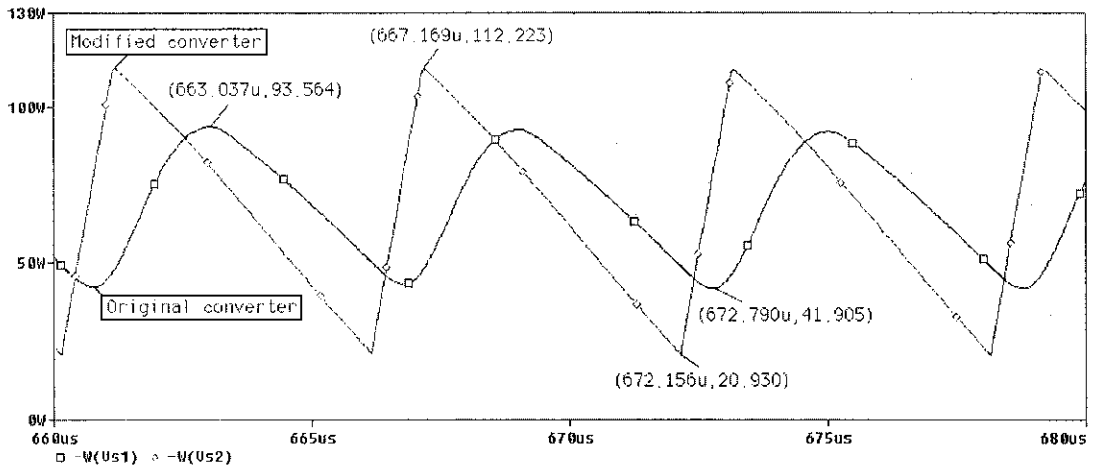
Figure 43: Waveforms of input power of the original boost converter [W(V$_{s1}$)] and of the modified boost converter [W(V$_{s2}$)]

The average input power of the original boost converter:

$$P_{in1} = W(V_{s1}) = \frac{93.564 + 41.905}{2} = 67.735W$$

The average input power of the modified boost converter:

$$P_{in2} = W(V_{s2}) = \frac{112.223 + 20.930}{2} = 66.577W$$

Figure 44 below shows the waveforms of output power of the original boost converter and the modified boost converter.

46
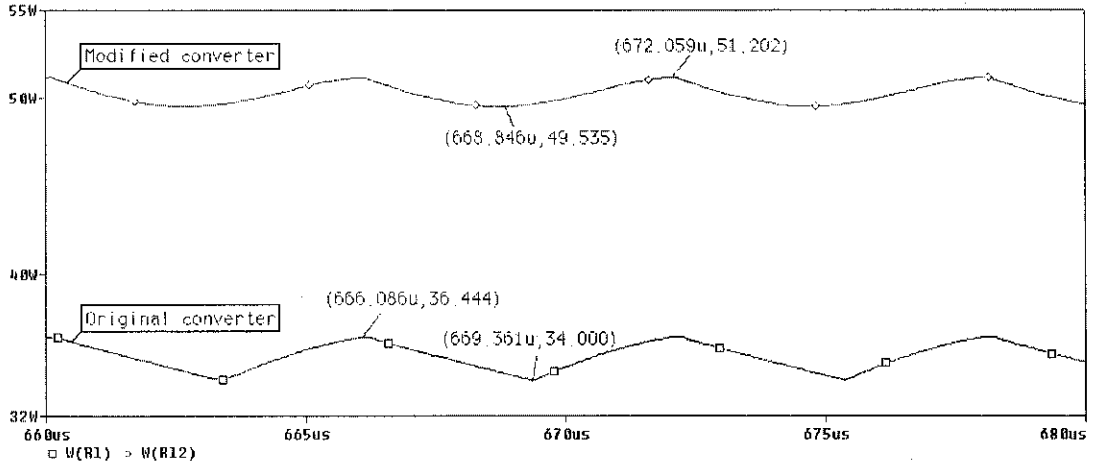
Figure 44: Waveforms of output power of the original boost converter [W(R₁)] and of the modified boost converter [W(R₁₂)]

Figure 44 shows that the average output power of the modified converter is greater than that of the original boost converter. It is because of the fact that the energy stored in the snubber inductor of the modified boost converter during the auxiliary switch turn-off is returned to the input or delivered to the output. Thus, the modified converter makes a more efficient use of input power. Following is the detailed calculations of average output power and power efficiency of the original converter and the modified converter with the active snubber:

The average output power of the original boost converter:

$$P_{out1} = W(V_{R1}) = \frac{36.444 + 34.000}{2} = 35.222W$$

The average output power of the original boost converter:

$$P_{out2} = W(V_{R12}) = \frac{51.202 + 49.535}{2} = 50.369W$$

The power efficiency of the original boost converter:

$$\eta_1 = \frac{P_{out1}}{P_{in1}} = \frac{W(R_1)}{W(V_{s1})} = \frac{35.222}{67.735} = 52.0\%$$

The power efficiency of the modified boost converter:

$$\eta_1 = \frac{P_{out2}}{P_{in2}} = \frac{W(R_{12})}{W(V_{s2})} = \frac{50.369}{66.577} = 75.6\%$$

47

Hence, the power efficiency increases from 52.0 % to 75.6 %, which gives an improvement of 45.4%.

4.1.3 Main switch performance

One of the major concerns on PWM design is the improvements in switch performance such as switching loss reduction, drain-to-source voltage ringing reduction, soft-switching characteristic optimization, and voltage stress minimization on switching transistor during switching transitions. In this study, the main switch performance is investigated in terms of drain-to-source voltage and switching power.

4.1.3.1 Main Switch Drain-to-Source Voltage

Figure 45 below shows the voltage waveforms of main switch drain-to-source and gate-to-source of the original boost converter and the modified boost converter with an active snubber:
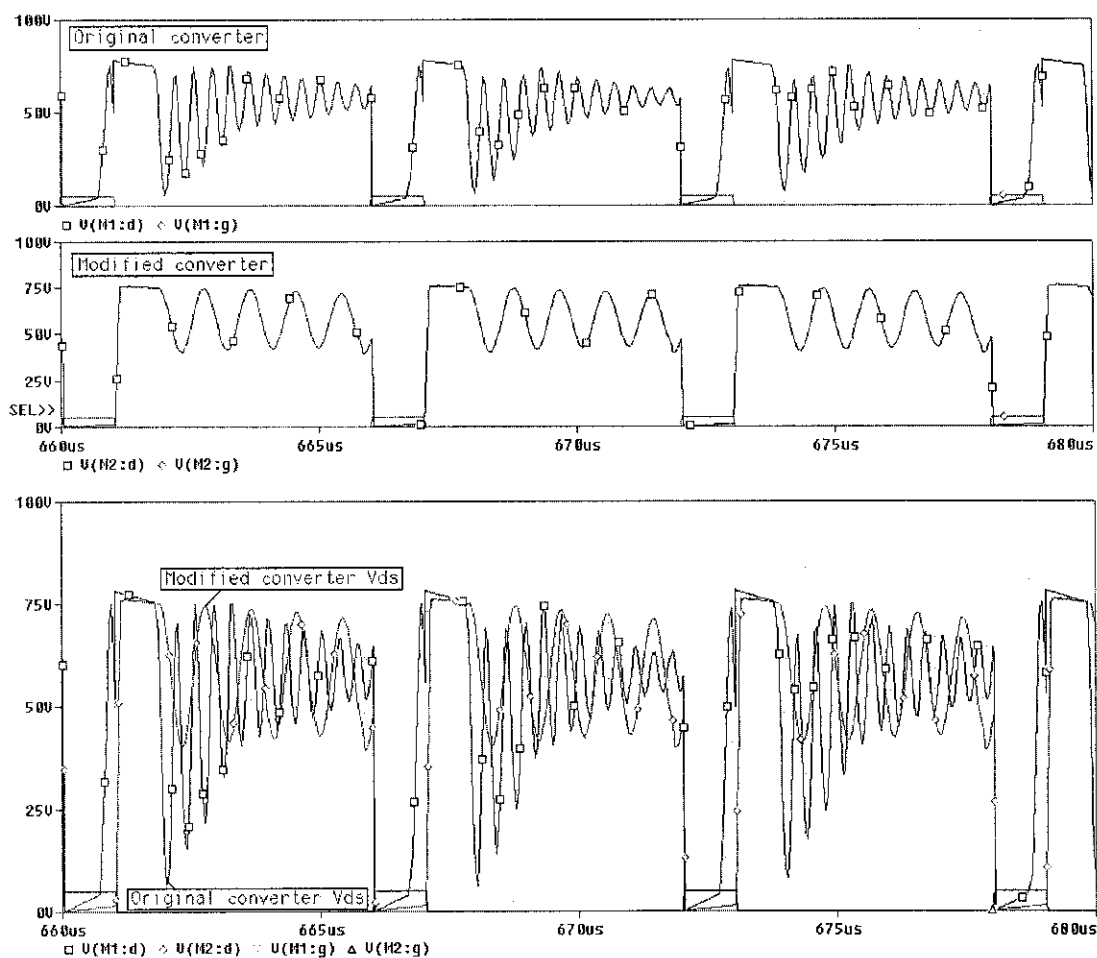
Figure 45: Waveforms of original boost converter's main switch gate-source voltage V_{gs1} **[V(M1:g)]**, main switch drain-to-source voltage V_{ds1} **[V(M1:d)]** and modified boost converter's main switch gate-source voltage V_{gs2} **[V(M2:g)]**, main switch drain-to-source voltage V_{ds2} **[V(M2:d)]**

Figure 45 shows that both the waveforms of V_{ds1} and V_{ds2} approach zero voltage during the main switch turn-on. However, the modified converter achieves better ZVS because V_{ds2} is closer to 0V. In other words, during the turn-on, the modified converter gives better soft-switching characteristic compared to the original converter.

During the main switch turn-off, the drain-to-source voltage waveform of the modified converter, V_{ds2}, shows less ringing components (4 ringing) compared to V_{ds1} of the original converter switch (12 ringing). Thus, it shows the reduction of voltage stress on

49

the main switch during switching transition. Moreover, the reduction in ringing shows the improvement in EMI performance of the converter has been made.

4.1.3.2 Switching Power of the Main Switch

Switching power loss is one of the major contributions to total power loss, which leads to low power efficiency. Let us analyze the main switch power waveforms of the original and the modified boost converter with an active snubber, which shown in **Figure 46**.
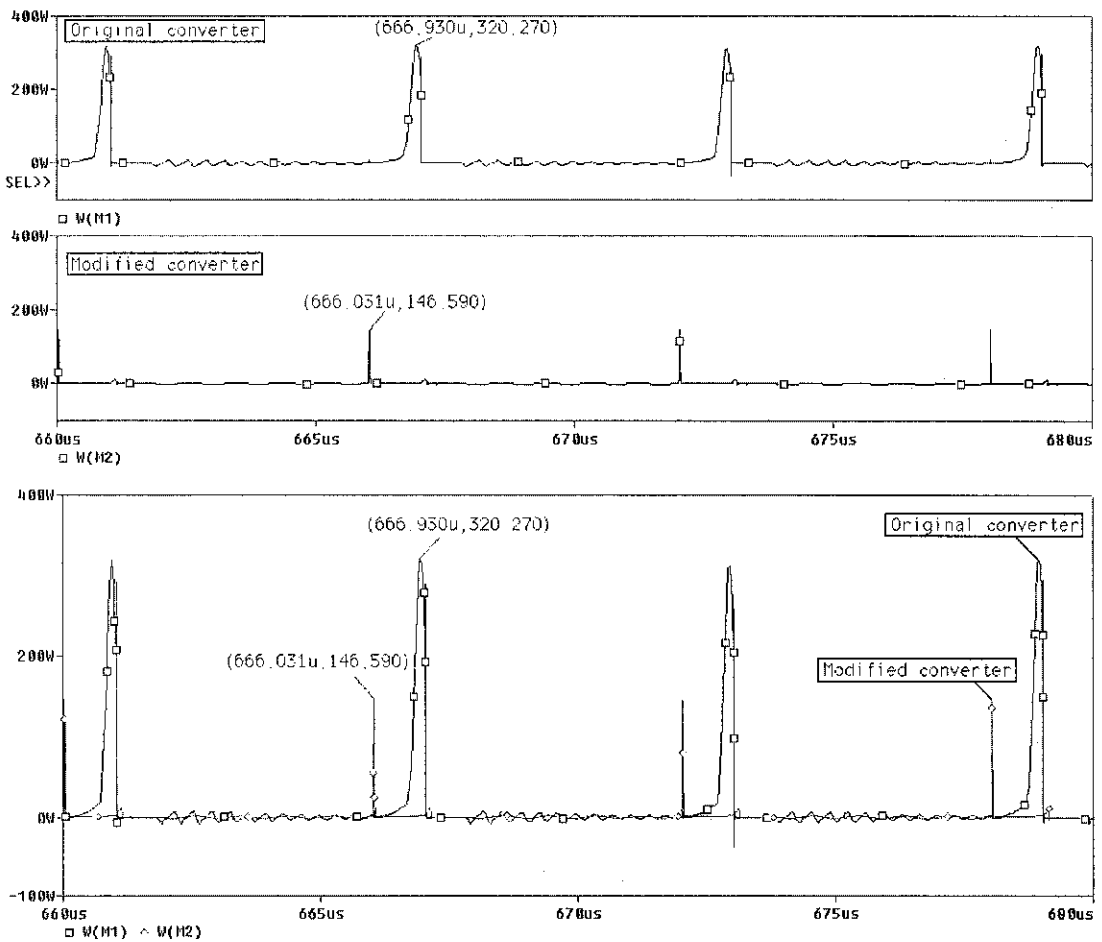
Figure 46: Waveforms of the power of the main switch in the original boost converter P_{M1} [**W(M1)**] and of the modified boost converter P_{M2} [**W(M2)**]

As shown in **Figure 46**, the spiking component of the main switch (main contribution to switching loss) during switching transition of the modified converter is much less than that of the original converter (reduced from 320.270 W to 146.590 W, improvement of more than 2 times). In other words, the switching loss during switching transition is reduced.

Figure 46 shows that the main switch power waveform of the original boost converter and the modified boost converter are out-of- phase. The modified boost converter employs an active snubber circuit consisting of a snubber inductor and a clamp capacitor. This LC tank in the active snubber causes the out-of-phase of the input current and thus the drain-to-source current, I_{ds}, of the modified converter and the original converter. That is the reason why the main switch power waveforms of the modified boost converter and the original converter are slightly out-of-phase.

4.1.4 Boost Rectifier Voltage

Figure 47 below shows the boost rectifier voltage waveforms of the original boost converter and the modified boost converter with an active snubber.
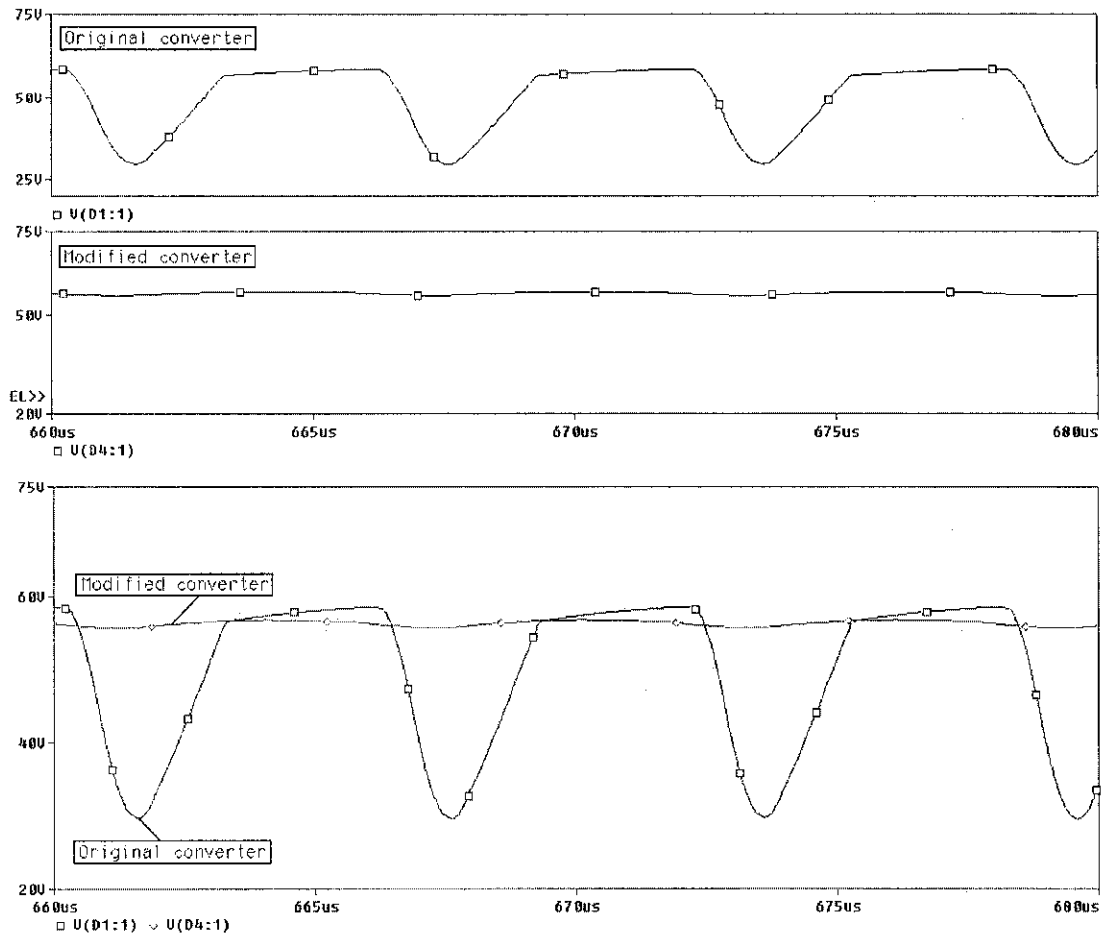
Figure 47: Waveforms of the boost rectifier voltage of the original boost converter [V(D$_1$:1)] and the modified boost converter [V(D$_4$:1)]

As shown in **Figure 47**, the boost rectifier voltage waveform of the modified boost converter [V(D$_4$:1)] is ringing free in comparison with the original boost converter [V(D$_1$:1)]. This is because of the effective clamping action of clamp diode D_c connected between the ground and the anode of the snubber diode, which is in series with the boost rectifier. The clamp diode D_c attempts to eliminate the parasitic ringing between the junction capacitance of the rectifier and the snubber inductor, the stress of the rectifier is thus minimized. As a result, the maximum reverse voltage across rectifier D_4 is equal to the output voltage.

4.2 Discussion

Based on the result analysis above, the modified soft-switched quasi-resonant DC/DC boost converter reduce the ringing of the drain-to-source voltage V_{ds}, thus reduce the voltage stress on the switching transistor during switching transitions, which is one of the common problem encountered in PWM design. The modified boost converter also eliminates the ringing of the boost rectifier voltage, thus the stress of the boost rectifier is minimized. In general, due to the significant reduction in ringing and abrupt transitions in the semiconductor voltage waveforms, the EMI performance of the converter has been improved. The switching power waveform shown in **Table 4** indicates the reduction in power loss of the switch during switching transitions. Importantly, the proposed design improves significantly the power efficiency. Last but not least, the output ripple voltage is reduced; therefore the DC output characteristic of boost converters has been improved. The following table below summaries the performance comparison of the modified soft-switched quasi-resonant DC/DC boost converter and the original converter in Ba-Thunya and Prasad's study:

Criterions	Original boost converter	Proposed boost converter
Power efficiency	52.0%	75.6%
Output ripple voltage	3.51%	1.88%
Ringing on V_{DS}	12 components/period	4 components/period
Switching loss	Higher	Reduced
Ringing on rectifier voltage	Present	Eliminated
Number of components	9	14

Table 4: Comparison of performance of the original boost converter and the modified boost converter

CHAPTER 5

CONCLUSION AND RECOMMENDATIONS

5.1 Conclusion

In this study, a novel soft-switched quasi-resonant DC/DC boost converter was proposed. The technique employs an active snubber circuit with an auxiliary switch and a clamp diode to reduce power losses in Ba-Thunya and Prasad's original soft-switched quasi-resonant DC/DC boost converter. The energy from the snubber inductor after the auxiliary switch turn-off is returned to the input or delivered to the output via the active snubber circuit, thus the voltage stress on the main switch is reduced and switching losses are minimized. Furthermore, the modified circuit reduces the reverse-recovery-related losses of the boost rectifier by controlling the *di/dt* rate of the rectifier current with the snubber inductor. By connecting a clamp diode between the ground and the anode of the snubber diode, it manages to eliminate the parasitic ringing between the junction capacitance of the boost rectifier and the snubber inductor, the stress of the boost rectifier is minimized. A modified soft-switched quasi-resonant boost converter with input voltage of 50V, 167 KHz switching frequency, duty ratio of 1/6 adopting this technique was simulated in PSPICE to verify the feasibility of the design. Performance analysis of the modified converter with an active snubber and a clamp diode was done in simulation to validate the improvements to the original soft-switched quasi-resonant DC/DC boost converter in Ba-Thunya and Prasad's study. The improvements include the increase in power efficiency, reduction in output ripple voltage, decrease in switching loss and stress minimization in the main switch during switching transitions and in the boost rectifier, thus the reduction in EMI radiation. The project has accomplished the objectives as followed:

54

1. To design a new technique to improve the performance of the most recent study of soft-switched quasi-resonant DC/DC boost converter (Ba-Thunya and Prasad's study).

2. To do simulation on the selected design.

Based on the simulation results, the new technique adopted in this study shows significant improvements of most common problems encountered in PWM design such as voltage stress on the switch and rectifier diode, power efficiency, switching loss, reverse-recovery-related losses, EMI radiation, and output voltage ripple. Last but not least, this study introduces a new, higher efficiency soft-switched quasi-resonant DC/DC boost converter, which is beneficial in industrial applications such as high-efficiency power supplies, direct-current motor drives electric vehicles (EV) and hybrid electric vehicles (HEV) systems.

5.2 Recommendations

There should be a few recommendations from what have been done in this project to further develop the study. Those recommendations are:

1. Implement the PCB circuit of the design to prove the simulation results

2. Apply the technique to topology of other soft-switched quasi-resonant DC/DC converters such as buck, buck-boost, fly-back, SEPIC and Cuk converters.

3. Further study on the design to improve performance of Ba-Thunya and Prasad's soft-switched quasi-resonant DC/DC boost converter with higher switching frequencies and higher voltage rating.

REFERENCES

[1] A.S. Ba-Thunya, S.K. Pillai and D. Prasad, "Some novel topologies of soft-switching quasi-resonant DC/DC converters with minimum voltage stress across the switch," *Industrial electronics Society IECON'98,* 1998, pp. 325-330.

[2] Y. Khersonsky, M. Robinson and D. Gutierrez, "New fast recovery diode technology cuts circuit losses, improves reliability," *Power Conversion & Intelligent Motion (PCIM) Magazine,* May 1992, pp. 16-25.

[3] J. Bassett, "New, zero voltage switching, high frequency boost converter topology for power factor correction," *Proc. International Telecommunication Energy Conf.,* 1995, pp. 813 – 820.

[4] C.M.C. Duarte and I. Barbi, "A new family of ZVS-PWM active-clamping DC-to-DC boost converters: analysis, design, and experimentation," *Proc. International Telecommunication Energy Conf.,* 1996, pp. 305-312.

[5] L.R. Barbosa, "A family of PWM soft-single-switched converters with low voltage and current stresses," *Proc. IEEE PESC' 97,* 1997, pp. 469-474.

[6] S.S. Ang, *Power Switching converter,* Marcel Dekker, Inc., 1998.

[7] I. Batarseh, *Power Electronic Circuits,* John Wiley & Sons, Inc., 2004.

[8] M. Bland, L. Empringham, J. Clare and P. Wheeler, "A new resonant soft-switching topology for direct AC/AC converters," *Power Electronics Specialists Conference, 2002. PESC 02.2002 IEEE 33rd Annual,* vol. 1, June 2002, pp 72-77.

[9] R.W. Erikson, A.F. Hernandez, A.F. Witulski, R. Xu, "A non-linear resonant switch," *Power Electronics Specialists Conference, 1989. PESC '89 Record, 20th Annual IEEE,* vol. 1, June 1989, pp. 43-50.

[10] B. Tomescu, "A unified approach to class E versus quasi-resonant switch topologies," *Circuits and Systems II: Express Briefs, IEEE Transaction on,* volume 45, issue 6, June 1998, pp.736-766.

[11] L. Hsiu, M. Goldman, R. Carlsten, A.F. Witulski and W. Kerwin, "Characterization and comparison of noise generation for quasi-resonant and pulse width modulated converters," *Power Electronics, IEEE Transactions on,* vol. 9, issue 4, July 1994, pp. 425-432.

[12] K. Laouamri, J.P. Ferrieux, C. Catellani and J. Barbaroux, "Modeling and analysis of wound integrated LCT structure for single stage resonant PFC rectifier," *Power Electronics, IEEE Transactions on,* vol. 18, issue 1, Jan. 2003, pp 256-269.

[13] C.T. Choi and C.K. Li, "Large signal modeling of quasi-resonant converters using regulated unified model," *Computers in Power Electronics, 200,. The 7th Workshop,* July 2000, pp. 132-138.

[14] A.F. Witulski, "Comparison of buck converter small signal dynamics pulse width modulated and quasi-resonant switches," *Applied Power Electronics Conference and Exposition, 1990. APEC'90, Conference Proceedings 1990, Fifth Annual,* 1990, pp. 195-204.

[15] S. Lungu, O. Pop and G. Chindris, "Educational platform for modeling of zero-voltage switching quasi-resonant boost converter," *Electronics Technology: Meeting the Challenges of Electronics Technology Progress, 2004., 27th International spring Seminar,* vol. 1, May 2004, pp. 147-152.

[16] B.T. Lin and Y.S. Lee, "A unified approach to modeling, synthesizing, and analyzing quasi-resonant converters," *Power Electronics, IEEE Transactions,* vol. 12, issue 6, Nov. 1997, pp. 983-992.

[17] K.T. Chau and A. Ioinovici, "Small-signal model of quasi-resonant converters in the presence of conduction losses," *Circuits and Systems 1991., IEEE International Symposium,* June 1991, pp. 1081-1084.

[18] C.C. Chong, C.Y. Chan and C.F. Foo, "A quasi-resonant converter-fed DC drive system," *Power Electronics and Applications, Fifth European Conference and Exposition, 1990. APEC '90. Conference Proceedings 1990., Fifth Annual,* March 1990, pp. 706-711.

[19] K. Yoshida, T. Ishi and N. Nagata, "Zero voltage switching approach for fly back converter," *INTELEC Conf. Proc.,* 1992, pp.324-329.

[20] K. Taniguchi, T. Yoshikawa, "Quasi-resonant PWM converter with high quality input waveforms and high efficiency," Proc. *IEEE PESC' 94,* 1994, pp. 1131-1136.

APPENDICES

APPENDIX A

DATASHEET FOR POWER DIODE (BAL74)

SOT23 HIGH SPEED SWITCHING DIODES

BAL74
BAR74

ISSUE 3 – FEBRUARY 1997

PIN CONFIGURATION

PARTMARKING DETAILS
BAL74 – JC
BAR74 – JB

BAL74   BAR74

SOT23
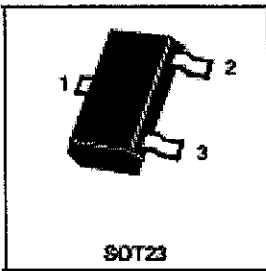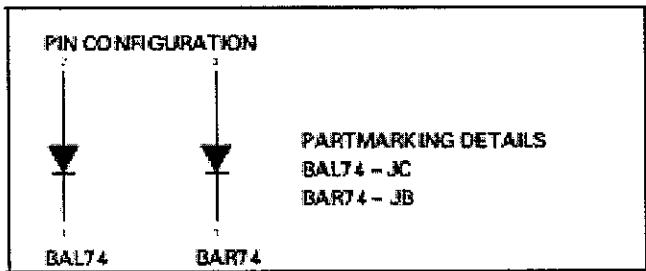
ABSOLUTE MAXIMUM RATINGS.

PARAMETER	SYMBOL	VALUE	UNIT
Continuous Reverse Voltage	V_R	50	V
Average Output Rectified Current (t_{av} = 10ms)	I_o	100	mA
Continuous Forward Current	I_F	150	mA
Peak Forward Current (t = 15ms)	I_{FM}	200	mA
Forward Surge Current (t = 1µs)	I_{FS}	1	A
Operating and Storage Temperature Range	T_j, T_{stg}	-65 to +150	°C
Power Dissipation at T_{amb} = 25°C	P_{tot}	330	mW

ELECTRICAL CHARACTERISTICS (at T_{amb} = 25°C unless otherwise stated).

PARAMETER	SYMBOL	MIN.	TYP.	MAX.	UNIT	CONDITIONS.
Breakdown Voltage	V_{BR}	51			V	I_R = 5µA
Forward Voltage	V_F			1.0	V	I_F = 100mA
Reverse current	I_R			0.1 100	µA µA	V_R = 50V V_R = 50V, T_{amb} = 125°C
Capacitance	C_o			2.0	pF	V_R = 0
Reverse Recovery Time	t_{rr}			4 2	ns ns	I_F = I_R = 10mA, I_{RR} = 1mA I_F = 10mA, V_R = 6V R_L = 100Ω

Spice parameter data is available upon request for this device

59

APPENDIX B

DATASHEET FOR POWER MOSFET (IRF843)

IRF840
IRF841
IRF842
IRF843

Part Number	V_{DSS}	$r_{DS(on)}$	I_D
IRF840	500 V	0.85 Ω	8.0 A
IRF841	450 V	0.85 Ω	8.0 A
IRF842	500 V	1.10 Ω	7.0 A
IRF843	450 V	1.10 Ω	7.0 A

N-CHANNEL ENHANCEMENT-MODE SILICON GATE TMOS POWER FIELD EFFECT TRANSISTOR

These TMOS Power FETs are designed for high voltage, high speed power switching applications such as switching regulators, converters, solenoid and relay drivers.

- Silicon Gate for Fast Switching Speeds
- Low $r_{DS(on)}$ to Minimize On-Losses. Specified at Elevated Temperature
- Rugged — SOA is Power Dissipation Limited
- Source-to-Drain Diode Characterized for Use With Inductive Loads

TMOS

MAXIMUM RATINGS

Rating	Symbol	IRF 840	IRF 841	IRF 842	IRF 843	Unit
Drain-Source Voltage	V_{DSS}	500	450	500	450	Vdc
Drain-Gate Voltage ($R_{GS} = 1.0$ mΩ)	V_{DGR}	500	450	500	450	Vdc
Gate-Source Voltage	V_{GS}	±20				Vdc
Drain Current Continuous Pulsed	I_D I_{DM}	8.0 32		7.0 28		Adc
Total Power Dissipation @ $T_C = 25°C$ Derate above 25°C	P_D	125 1.0				Watts W/°C
Operating and Storage Temperature Range	T_J, T_{stg}	−55 to 150				°C

THERMAL CHARACTERISTICS

Thermal Resistance Junction to Case Junction to Ambient	$R_{\theta JC}$ $R_{\theta JA}$	1.0 62.5	°C/W
Maximum Lead Temp. for Soldering Purposes, 1/8" from Case for 5 Seconds	T_L	275	°C

See the MTP8N40 Designer's Data Sheet for a complete set of design curves for the product on this data sheet.

The Designer's Data Sheet permits the design of most circuits entirely from the information presented. Limit curves — representing boundaries on device characteristics — are given to facilitate "worst case" design.

CASE 221A-04
TO-220AB

60

ELECTRICAL CHARACTERISTICS (T_C = 25°C unless otherwise noted)

Characteristic	Symbol	Min	Max	Unit
OFF CHARACTERISTICS				
Drain-Source Breakdown Voltage	$V_{(BR)DSS}$		—	Vdc
(V_GS = 0, I_D = 0.25 mA) IRF841, IRF843		450	—	
IRF840, IRF842		500	—	
Zero Gate Voltage Drain Current	I_{DSS}			mAdc
(V_DS = Rated V_DSS, V_GS = 0)		—	0.25	
(V_DS = 0.8 Rated V_DSS, V_GS = 0, T_J = 125°C)		—	1.00	
Gate-Body Leakage Current, Forward	I_{GSF}	—	500	nAdc
(V_GSF = 20 Vdc, V_DS = 0)				
Gate-Body Leakage Current, Reverse	I_{GSR}	—	500	nAdc
(V_GSR = 20 Vdc, V_DS = 0)				
ON CHARACTERISTICS*				
Gate Threshold Voltage	$V_{GS(th)}$	2.0	4.0	Vdc
(V_DS = V_GS, I_D = 0.25 mA)				
Static Drain-Source On-Resistance	$r_{DS(on)}$			Ohm
(V_GS = 10 Vdc, I_D = 4.0 Adc) IRF840, IRF841		—	0.85	
IRF842, IRF843		—	1.0	
On-State Drain Current (V_GS = 10 V)	$I_{D(on)}$			Adc
(V_DS ≥ 6.8 Vdc) IRF840, IRF841		8.0	—	
(V_DS ≥ 7.0 Vdc) IRF842, IRF843		7.0	—	
Forward Transconductance	g_{FS}			mhos
(V_DS ≥ 6.8 V, I_D = 4.0 A) IRF840, IRF841		4.0	—	
(V_DS ≥ 7.0 V, I_D = 4.0 A) IRF842, IRF843		4.0	—	
DYNAMIC CHARACTERISTICS				
Input Capacitance	C_{iss}	—	1600	pF
Output Capacitance	C_{oss}	—	350	
Reverse Transfer Capacitance	C_{rss}	—	150	
SWITCHING CHARACTERISTICS*				
Turn-On Delay Time	$t_{d(on)}$	—	35	ns
Rise Time	t_r	—	15	
Turn-Off Delay Time	$t_{d(off)}$	—	90	
Fall Time	t_f	—	30	
Total Gate Charge	Q_g	40 (Typ)	60	nC
Gate-Source Charge	Q_{gs}	20 (Typ)	—	
Gate-Drain Charge	Q_{gd}	20 (Typ)	—	
SOURCE DRAIN DIODE CHARACTERISTICS*				
Forward On-Voltage	V_{SD}	—	1.9 (1)	Vdc
Forward Turn-On Time	t_{on}	Limited by stray inductance		
Reverse Recovery Time	t_{rr}	600 (Typ)	—	ns
INTERNAL PACKAGE INDUCTANCE (TO-220)				
Internal Drain Inductance	L_d		—	nH
(Measured from the contact screw on tab to center of die)		3.5 (Typ)	—	
(Measured from the drain lead 0.25" from package to center of die)		4.5 (Typ)	—	
Internal Source Inductance	L_s	7.5 (Typ)	—	
(Measured from the source lead 0.25" from package to source bond pad)				

Dynamic Characteristics conditions: (V_DS = 25 V, V_GS = 0, f = 1.0 MHz)

Switching Characteristics conditions: (V_DD = 200 V, I_D = 4.0 Aps, R_gen = 4.7 Ohms)

Gate Charge conditions: (V_GS = 10 V, V_DS = 0.8 × Rated V_DSS, I_D = Rated I_D)

Source Drain Diode conditions: (I_S = Rated I_D, V_GS = 0)

*Pulse Test: Pulse Width ≤ 300 μs, Duty Cycle ≤ 2.0%.
(1) Add 0.1 V for IRF840 and IRF841.

61

APPENDIX C

DATASHEET FOR RECTIFIER (MUR860)

FAIRCHILD
SEMICONDUCTOR®

MUR840, MUR860, RURP840, RURP860

8A, 400V - 600V Ultrafast Diodes

The MUR840, MUR860, RURP840 and RURP860 are low forward voltage drop ultrafast recovery rectifiers ($t_{rr} < 60ns$). They use a glass-passivated ion-implanted, epitaxial construction.

These devices are intended for use as output rectifiers and flywheel diodes in a variety of high-frequency pulse-width modulated switching regulators. Their low stored charge and attendant fast reverse-recovery behavior minimize electrical noise generation and in many circuits markedly reduce the turn-on dissipation of the associated power switching transistors.

Formerly developmental type TA09616.

Ordering Information

PART NUMBER	PACKAGE	BRAND
MUR840	TO-220AC	MUR840
RURP840	TO-220AC	RURP840
MUR860	TO-220AC	MUR860
RURP860	TO-220AC	RURP860

NOTE: When ordering, use the entire part number.

Symbol

K

A

Features

- Ultrafast with Soft Recovery . . . . <60ns
- Operating Temperature. . . . . .175°C
- Reverse Voltage 600V
- Avalanche Energy Rated
- Planar Construction

Applications

- Switching Power Supplies
- Power Switching Circuits
- General Purpose

Packaging

JEDEC TO-220AC

ANODE
CATHODE
CATHODE
(FLANGE)

Absolute Maximum Ratings $T_C = 25°C$, Unless Otherwise Specified

		MUR840 RURP840	MUR860 RURP860	UNITS
Peak Repetitive Reverse Voltage	V_{RRM}	400	600	V
Working Peak Reverse Voltage	V_{RWM}	400	600	V
DC Blocking Voltage	V_R	400	600	V
Average Rectified Forward Current . . . . ($T_C = 155°C$)	$I_{F(AV)}$	8	8	A
Repetitive Peak Surge Current . . . . (Square Wave, 20kHz)	I_{FRM}	16	16	A
Nonrepetitive Peak Surge Current . . . . (Halfwave, 1 Phase, 60Hz)	I_{FSM}	100	100	A
Maximum Power Dissipation	P_D	75	75	W
Avalanche Energy (See Figures 10 and 11)	E_{AVL}	20	20	mJ
Operating and Storage Temperature	T_{STG}, T_J	-65 to 175	-65 to 175	°C
Maximum Lead Temperature for Soldering				
Leads at 0.063 in. (1.6mm) from case for 10s	T_L	300	300	°C
Package Body for 10s, see Tech Brief 334.	T_{PKG}	260	260	°C

Electrical Specifications $T_C = 25°C$, Unless Otherwise Specified

SYMBOL	TEST CONDITION	MUR840, RURP840			MUR860, RURP860			UNITS
		MIN	TYP	MAX	MIN	TYP	MAX	
V_F	$I_F = 8A$	-	-	1.3	-	-	1.5	V
	$I_F = 8A, T_C = 150°C$	-	-	1.0	-	-	1.2	V
I_R	$V_R = 400V$	-	-	100	-	-	-	μA
	$V_R = 600V$	-	-	-	-	-	100	μA
	$V_R = 400V, T_C = 150°C$	-	-	500	-	-	-	μA
	$V_R = 600V, T_C = 150°C$	-	-	-	-	-	500	μA
t_{rr}	$I_F = 1A, dI_F/dt = 200A/μs$	-	-	60	-	-	60	ns
	$I_F = 8A, dI_F/dt = 200A/μs$	-	-	70	-	-	70	ns
t_a	$I_F = 8A, dI_F/dt = 200A/μs$	-	32	-	-	32	-	ns
t_b	$I_F = 8A, dI_F/dt = 200A/μs$	-	21	-	-	21	-	ns
Q_{RR}	$I_F = 8A, dI_F/dt = 200A/μs$	-	195	-	-	195	-	nC
C_J	$V_R = 10V, I_F = 0A$	-	25	-	-	25	-	pF
$R_{θJC}$		-	-	2	-	-	2	°C/W

DEFINITIONS

V_F = Instantaneous forward voltage (pw = 300μs, D = 2%).

I_R = Instantaneous reverse current.

t_{rr} = Reverse recovery time (See Figure 9), summation of $t_a + t_b$.

t_a = Time to reach peak reverse current (See Figure 9).

t_b = Time from peak I_{RM} to projected zero crossing of I_{RM} based on a straight line from peak I_{RM} through 25% of I_{RM} (See Figure 9).

Q_{RR} = Reverse recovery charge.

C_J = Junction Capacitance.

$R_{θJC}$ = Thermal resistance junction to case.

pw = pulse width.

D = duty cycle.

Typical Performance Curves
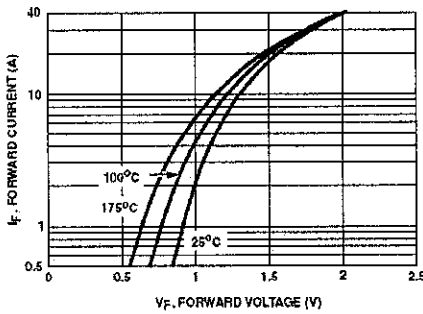
FIGURE 1. FORWARD CURRENT vs FORWARD VOLTAGE
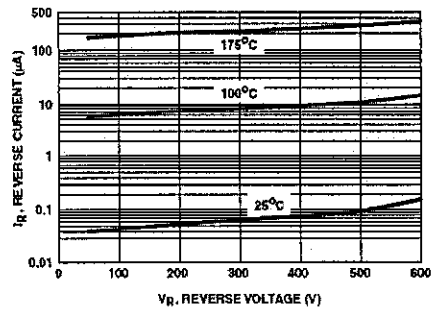
FIGURE 2. REVERSE CURRENT vs REVERSE VOLTAGE

APPENDIX D
LIST OF COMPONENTS

Quantity	Description
2	Power MOSFET (N-channel) – IRF843
1	Rectifier – MUR860
5	Power Diode – BAL74
1	Power inductor – 27 μH
1	Power inductor – 9 μH
2	Power capacitor – 0.1 μF
1	Power capacitor – 1 μF
1	Power resistor – 92 Ω

APPENDIX E
TECHNICAL REPORT

IMPROVEMENT STUDY OF SOFT-SWITCHED

QUASI-RESONANT DC/DC BOOST CONVERTER

Tran Minh Dung, Nor Zaihar Yahaya

School of Electrical and Electronic Engineering
Universiti Teknologi Petronas, Bandar Seri Iskandar,
31750 Tronoh, Perak Darul Ridzuan, Malaysia.
Tel: +60-175209049
E-mail: *tranminhdung@gmail.com, norzaihar_yahaya@petronas.com.my*

Abstract

This paper describes a novel soft-switched quasi-resonant DC/DC boost converter. Recently, remarkable efforts have been made in soft-switched quasi-resonant DC/DC converters to reduce losses and improve power efficiency. This project presents a new technique and it had improved the performance of the most recent study on soft-switched quasi-resonant DC/DC boost converter, which is presented in Ba-Thunya and Prasad's study [1]. The proposed converter employs an active snubber circuit with an auxiliary switch in series with a clamp capacitor to reduce power losses in Ba-Thunya and Prasad's original an active snubber circuit with an auxiliary switch and a clamp diode to reduce power losses in Ba-Thunya and Prasad's original converter. The energy from the snubber inductor after the auxiliary switch turn-off is returned to the input or delivered to the output via the active snubber circuit, thus the voltage stress on the main switch is reduced and switching losses are minimized. Furthermore, the proposed converter reduces the reverse-recovery-related losses of the boost rectifier by controlling the di/dt rate of the rectifier current with the snubber inductor. This report describes the principle of operation of the new soft-switched quasi-resonant DC/DC boost converter. The feasibility study of the proposed converter is investigated using PSPICE program.

Keywords:

Quasi-resonance, Boost Converter and Active Snubber

Introduction

In recent years, significant research and development efforts have been made in soft-switched quasi-resonant DC/DC converters to reduce losses and to increase the switching frequency. Soft-switched quasi-resonant DC/DC converters having increased efficiency, low cost, high power operation and reduced weight as well as size have been produced to give applications in industry such as high-power high-efficiency power supplies, direct-current motor drives electric vehicles (EV) and hybrid electric vehicles (HEV) systems [1]-[4].

The major thrust in soft-switched quasi-resonant DC/DC boost converter improvement study is to reduce losses and to increase the switching frequency. The current proposed circuit of Ba-Thunya and Prasad's study, which use two coupled inductors with clamp capacitor for the resonant circuit (shown in *Figure 1*) [1], [5], [6] provides a valuable solution to achieve high switching frequency, and allow zero voltage and zero current switching for turning off the control switch and zero current switching for turning it on. The main drawback of this converter is the voltage stresses on the control switch and boost rectifier [7]-[10].

Furthermore, at high output voltage, the converter requires the use of a fast-recovery boost rectifier. At high switching frequencies, fast-recovery rectifiers produce significant reverse-recovery-related losses when switched under "hard-switched" conditions [11], this leads to high total power loss and low power efficiency. This project focuses on modifying the soft-switched quasi-resonant DC/DC boost converter by using an active snubber circuit consisting of an auxiliary switch in series with a clamp capacitor [12]-[14]. In addition, a clamp diode is connected between the ground and the anode of the snubber diode, which is in series with the boost rectifier. The proposed design provides a means for the energy from the inductor in series with the main switch after the switch turn-off is returned to the input to deliver to the output via the active snubber circuit, thus reduces the voltage stress on the main switch and reduce the switching loss. Furthermore, the clamp diode effect is to eliminate the parasitic ringing between the junction capacitance of the rectifier and the inductor in series with the main switch, the stress of the rectifier is then minimized [15]-[17].
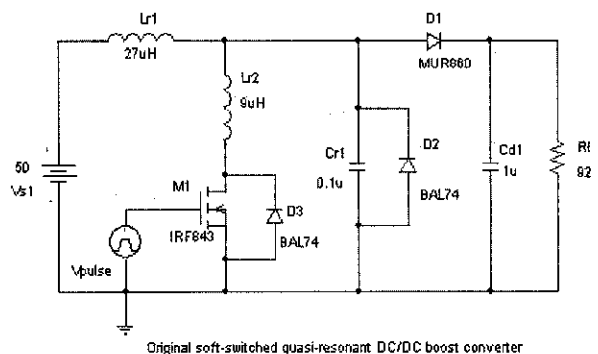
Original soft-switched quasi-resonant DC/DC boost converter

Figure 1- Original quasi-resonant soft-switched DC/DC boost converter using two coupled inductors with capacitor

In this project, an active snubber circuit consisting of a clamp capacitor in series with an auxiliary switch and a snubber inductor is employed. The snubber inductor controls the *di/dt* rate of the boost rectifier during its turn-off [18], [19]. The energy from the snubber inductor after the main switch turn-off is returned to the input or delivered to the output via the active snubber. In addition, a clamp diode is connected between the ground and the anode of the snubber diode D_s [20], which is in series with boost rectifier in order to eliminate the parasitic ringing between the junction capacitance of the boost rectifier and the snubber inductor, the stress of the boost rectifier is minimized. *Figure 2* below shows the combination of the snubber circuit and clamp capacitor:
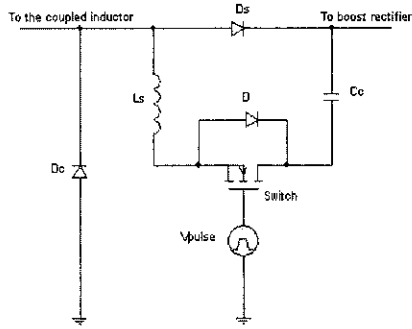
Figure 2- Combination of the active snubber circuit and a clamp capacitor

The combination of the active snubber circuit and a clamp capacitor is added into the original soft-switched quasi-resonant DC/DC boost converter in order to improve the efficiency, reduce the voltage stress on the main switch and the boost rectifier, and thus improve the EMI performance of the original circuit. The circuit diagram of the modified soft-switched quasi-resonant converter with active snubber and a diode is shown in *Figure 3*.
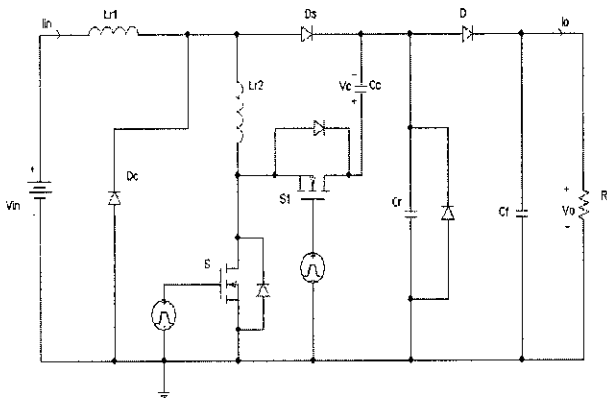
Figure 3- The proposed boost converter

Circuit Operation

To simplify the analysis of operation, it is assumed that the inductance of boost inductor L_{r1} is large so that it can be represented by constant-current source I_{in}, and the

output-ripple voltage is negligible so that the voltage across the output filter capacitor can be represented by constant-voltage source V_o. In addition, it is assumed that in the on-state, semiconductors exhibit zero resistance, i.e., they are short circuits. However, the output capacitances of the MOSFETs and the reverse-recovery charge of the rectifier are not neglected in this analysis. To further facilitate the explanation of operation, *Figure 4* shows topological stages of the circuit during a switching cycle. It should be noted that because the junction capacitance of boost rectifier D_s has been neglected for the time being and the clamp diode D_c is not shown in *Figure 4* since it never conducts.
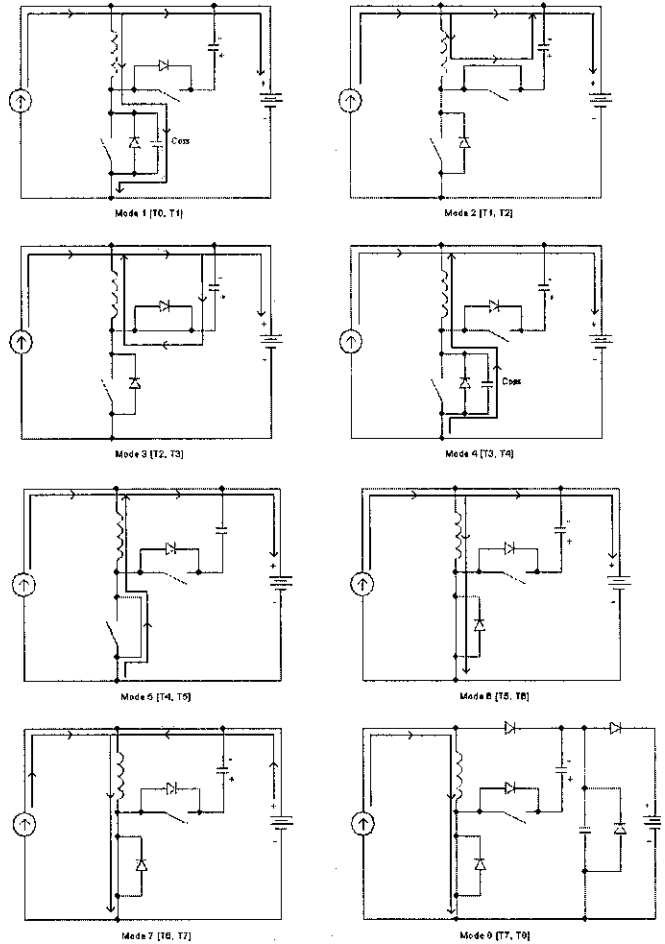
Figure 4- Operation modes

Mode 1 [T_0, T_1]

Mode 1 begins at $t = T_o$, when the main switch S is turned off. The entire input current I_{in} flows through inductor L_{r2} and switch S. At the same time, rectifier D_s is off with a reverse voltage across its terminals equal to output voltage V_o. Auxiliary switch S_1 is also off, blocking the voltage $V_o + V_c$, where V_c is the voltage across the clamp capacitor and V_o is the output voltage.

Mode 2 [T_1, T_3]

Mode 2 begins at $t = T_1$. During mode 2 inductor current i_{Lr1} continues to decrease as it discharges to clamp capacitor C_c.

If the capacitance of the C_c is large, capacitor voltage v_c is almost constant and inductor current i_{Lr1} decrease linearly. This topological stage ends at $t = T_3$, when i_{Lr1} reaches zero and the antiparallel diode of auxiliary switch S_1 stops conducting. To achieve ZVS of S_1, it is necessary to turn on the transistor of switch $S1$ before $t = T_3$, i.e., while its antiparallel diode is conducting. The MOSFET of switch S_1 is turned on at $t = T_2$ (T_2 is in between [T_1, T_3]).

Mode 3 [T_3, T_4]

Mode 3 begins at $t = T_3$. The transistor of switch S_1 is turned on prior to $t = T_3$, inductor current i_{Lr1} will continue to flow after $t = T_3$ in the opposite direction through the closed transistor. This interval ends at $t = T_4$ when auxiliary switch is turned off.

Mode 4 [T_4, T_5]

Assuming that inductor energy is more than enough to discharge C_{oss} to zero, v_s will reach zero at $t = T_5$, while inductor current i_{Lr1} is still negative. Mode 4 ends at $t = T_5$.

Mode 4 starts at $t = T_4$ when the switch S_1 is turned off, conductor current i_{Lr1} can not flow anymore through clamp capacitor C_c.

Mode 5 [T_5, T_6]

Mode 5 starts at $t = T_5$, when v_s reaches zero while inductor current i_{Lr1} is still negative. As a result, the antiparallel diode of S will start conducting. To achieve ZVS of switch S, it is necessary to turn on the transistor of switch S during interval [T_5, T_6] when the antiparallel diode of S id turned on during this interval, i_{Lr1} will continue to increase linearly after $t = T_6$

Mode 6 [T_6, T_7]

Mode 6 begins at $t = T_6$. After this time, the inductor current i_{Lr1} continues to increase linearly from the previous stage. At the same time, snubber diode i_{Ds} will continue to decrease linearly. The mode ends at $t = T_7$, when i_{Lr1} reaches the input-current level I_{in}, and the snubber diode current i_{Ds} falls to zero.

Mode 7 [T_7, T_8]

Mode 7 begins at $t = T_7$, when the inductor current i_{Lr1} increases linearly to the input-current level I_{in}, and the snubber diode current i_{Ds} falls to zero

This mode ends at $t = T_8$ when the junction capacitance of the snubber diode affects the circuit operation after the snubber diode D_s has recovered at $t = T_8$.

Mode 8 [T_8, T_9]

Mode 8 begins at $t = T_8$, when the junction capacitance of the snubber diode D_s affects the circuit operation after snubber diode has recovered. Once the snubber diode has recovered, the entire input current I_{in} flows through switch S until the next switching cycle is initiated at $t = T_9$.

Result

The PSPICE simulation shows the performance result of the original boost converter and the modified boost converter. Details as follows:

a) Output ripple voltage
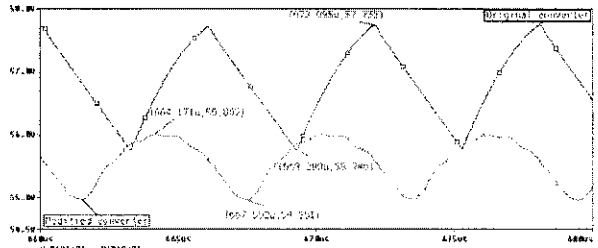
Figure 5- Output ripple voltage of the original boost converter [V(Rl:2)] and the modified boost converter with an active snubber [V(Rl2:2)]

The output ripple voltage of the original boost converter:

$$V_{out1(ripple)} = \frac{57.735 - 55.746}{(57.735 + 55.746)/2} = 3.51\%$$

The output ripple voltage of the modified boost converter:

$$V_{out2(ripple)} = \frac{56.002 - 54.961}{(56.002 + 54.961)/2} = 1.88\%$$

The modified boost converter with a snubber circuit introduces an improvement in the output ripple voltage (decrease from 3.51 % to 1.88 %), improvement of 46.4 %. Hence, the DC output characteristic of the converter has been improved.

b) Power Efficiency
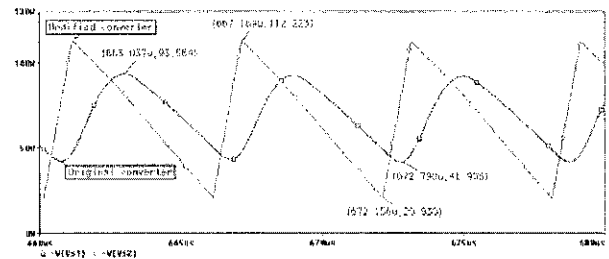
Figure 6- Input power of the original boost converter [W(V_{s1})] and of the modified boost converter [W(V_{s2})]
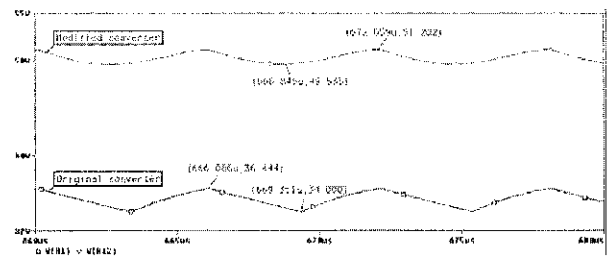
Figure 7-Output power of the original boost converter [W(R_1)] and of the modified boost converter [W(R_{12})]

Figure 7 shows that the average output power of the modified converter is greater than that of the original boost converter. It is because of the fact that the energy stored in the snubber inductor of the modified boost converter during the auxiliary switch turn-off is returned to the input or delivered to the output.

The power efficiency of the original boost converter:

$$\eta_1 = \frac{P_{out1}}{P_{in1}} = \frac{W(R_1)}{W(V_{s1})} = \frac{(36.444 + 34.000)/2}{(93.564 + 41.905)/2} = 52.0\%$$

The power efficiency of the modified boost converter:

$$\eta_2 = \frac{P_{out2}}{P_{in2}} = \frac{W(R_{l2})}{W(V_{s2})} = \frac{(51.202 + 49.535)/2}{(112.223 + 20.930)/2} = 75.6\%$$

Hence, the efficiency is increased from 52.7% to 75.6%

c) Main switch performance
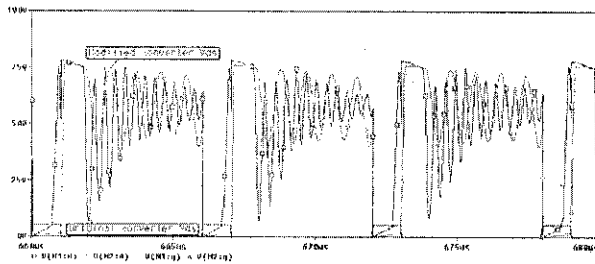
Figure 8- Waveforms of original boost converter's main switch gate-source voltage V_{gs1} [V(M1:g)], main switch drain-to-source voltage V_{ds1} [V(M1:d)] and original boost converter's main switch gate-source voltage V_{gs2} [V(M2:g)], main switch drain-to-source voltage V_{ds2} [V(M2:d)]

Figure 8 shows that both the waveforms of V_{ds1} and V_{ds2} approach zero voltage during the main switch turn-on. However, the modified converter achieves better ZVS because V_{ds2} is closer to 0V. In other words, during the turn-on, the modified converter gives better soft-switching characteristic compared to the original converter.

During the main switch turn-off, the drain-to-source voltage waveform of the modified converter, V_{ds2}, shows less ringing components (4 ringing) compared to V_{ds1} of the original converter switch (12 ringing). Thus, it shows the reduction of voltage stress on the main switch during switching transition. Moreover, the reduction in ringing shows the improvement in EMI performance of the converter has been made.

Let us analyze the main switch power waveforms of the original and the modified boost converter with a snubber circuit.
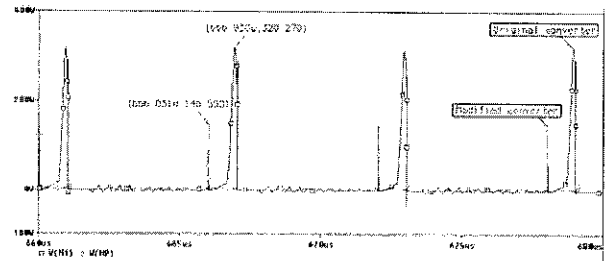
Figure 9- Waveforms of the power of the main switch in the original boost converter P_{M1} [W(M1)] and of the modified boost converter P_{M2} [W(M2)]

As shown in *Figure 9*, the spiking component of the main switch (main contribution to switching loss) during switching transition of the modified converter is much less than that of the original converter (reduced from 320.270 W to 146.590 W, improvement of more than 2 times). In other words, the switching loss during switching transition is reduced.

d) Boost Rectifier Voltage
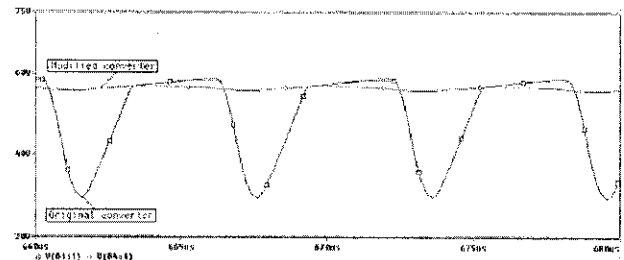
Figure 10- Waveforms of the boost rectifier voltage of the original boost converter [V(D_1:1)] and the modified boost converter [V(D_4:1)]

As shown in **Figure 47**, the boost rectifier voltage waveform of the modified boost converter [V(D_4:1)] is ringing free in comparison with the original boost converter [V(D_1:1)]. This is because of the effective clamping action of clamp diode D_c connected between the ground and the anode of the snubber diode, which is in series with the boost rectifier. The clamp diode D_c attempts to eliminate the parasitic ringing between the junction capacitance of the rectifier and the snubber inductor, the stress of the rectifier is thus minimized. As a result, the maximum reverse voltage across rectifier D_4 is equal to the output voltage.

Discussion

Based on the result analysis above, the modified soft-switched quasi-resonant DC/DC boost converter reduce the ringing of the drain-to-source voltage V_{ds} thus reduce the voltage stress on the switching transistor during switching transitions, which is one of the common problem encountered in PWM design. The modified boost converter also eliminates the ringing of the boost rectifier voltage, thus the stress of the boost rectifier is minimized. In general, due

to the significant reduction in ringing and abrupt transitions in the semiconductor voltage waveforms, the EMI performance of the converter has been improved. The switching power waveform shown in **Table 4** indicates the reduction in power loss of the switch during switching transitions. Importantly, the proposed design improves significantly the power efficiency. Last but not least, the output ripple voltage is reduced; therefore the DC output characteristic of boost converters has been improved. The following table below summaries the performance comparison of the modified soft-switched quasi-resonant DC/DC boost converter and the original converter in Ba-Thunya and Prasad's study:

Criterions	Original boost converter	Proposed boost converter
Power efficiency	52.0%	75.6%
Output ripple voltage	3.51%	1.88%
Ringing on V_{DS}	12 components/period	4 components/period
Switching loss	Higher	Reduced
Ringing on rectifier voltage	Present	Eliminated
Number of components	9	14

Table 1- Comparison of performance of the original boost converter and the modified boost converter

Conclusion

In this study, a novel soft-switched quasi-resonant DC/DC boost converter was proposed. The technique employs an active snubber circuit with an auxiliary switch and a clamp diode to reduce power losses in Ba-Thunya and Prasad's original soft-switched quasi-resonant DC/DC boost converter. The energy from the snubber inductor after the auxiliary switch turn-off is returned to the input or delivered to the output via the active snubber circuit, thus the voltage stress on the main switch is reduced and switching losses are minimized. Furthermore, the modified circuit reduces the reverse-recovery-related losses of the boost rectifier by controlling the di/dt rate of the rectifier current with the snubber inductor. By connecting a clamp diode between the ground and the anode of the snubber diode, it manages to eliminate the parasitic ringing between the junction capacitance of the boost rectifier and the snubber inductor, the stress of the boost rectifier is minimized. A modified soft-switched quasi-resonant boost converter with input voltage of 50V, 167 KHz switching frequency, duty ratio of 1/6 adopting this technique was simulated in PSPICE to verify the feasibility of the design. Performance analysis of the modified converter with an active snubber and a clamp

diode was done in simulation to validate the improvements to the original soft-switched quasi-resonant DC/DC boost converter in Ba-Thunya and Prasad's study. The improvements include the increase in power efficiency, reduction in output ripple voltage, decrease in switching loss and stress minimization in the main switch during switching transitions and in the boost rectifier, thus the reduction in EMI radiation. Last but not least, this study introduces the new lower-cost, higher efficiency power soft-switched quasi-resonant DC/DC boost converter, which is beneficial in industrial applications such as high-efficiency power supplies, direct-current motor drives electric vehicles (EV) and hybrid electric vehicles (HEV) systems.

Acknowledgement

Reference

[1] A.S. Ba-Thunya, S.K. Pillai and D. Prasad, "Some novel topologies of soft-switching quasi-resonant DC/DC converters with minimum voltage stress across the switch," *Industrial electronics Society IECON'98*, 1998, pp. 325-330.

[2] Y. Khersonsky, M. Robinson and D. Gutierrez, "New fast recovery diode technology cuts circuit losses, improves reliability," *Power Conversion & Intelligent Motion (PCIM) Magazine*, May 1992, pp. 16-25.

[3] J. Bassett, "New, zero voltage switching, high frequency boost converter topology for power factor correction," *Proc. International Telecommunication Energy Conf.*, 1995, pp. 813 – 820.

[4] C.M.C. Duarte and I. Barbi, "A new family of ZVS-PWM active-clamping DC-to-DC boost converters: analysis, design, and experimentation," *Proc. International Telecommunication Energy Conf.*, 1996, pp. 305-312.

[5] L.R. Barbosa, "A family of PWM soft-single-switched converters with low voltage and current stresses," *Proc. IEEE PESC'97*, 1997, pp. 469-474.

[6] S.S. Ang, *Power Switching converter*, Marcel Dekker, Inc., 1998.

[7] I. Batarseh, *Power Electronic Circuits*, John Wiley & Sons, Inc., 2004.

[8] M. Bland, L. Empringham, J. Clare and P. Wheeler, "A new resonant soft-switching topology for direct AC/AC converters," *Power Electronics Specialists Conference, 2002. PESC 02.2002 IEEE 33rd Annual*, vol. 1, June 2002, pp 72-77.

[9] R.W. Erikson, A.F. Hernandez, A.F. Witulski, R. Xu, "A non-linear resonant switch," *Power Electronics Specialists Conference, 1989. PESC '89 Record, 20th Annual IEEE*, vol. 1, June 1989, pp. 43-50.

[10] B. Tomescu, "A unified approach to class E versus quasi-resonant switch topologies," *Circuits and Systems II: Express Briefs, IEEE Transaction on*, volume 45, issue 6, June 1998, pp.736-766.

[11] L. Hsiu, M. Goldman, R. Carlsten, A.F. Witulski and W. Kerwin, "Characterization and comparison of noise generation for quasi-resonant and pulse width modulated converters," *Power Electronics, IEEE Transactions on,* vol. 9, issue 4, July 1994, pp. 425-432.

[12] K. Laouamri, J.P. Ferrieux, C. Catellani and J. Barbaroux, "Modeling and analysis of wound integrated LCT structure for single stage resonant PFC rectifier," *Power Electronics, IEEE Transactions on,* vol. 18, issue 1, Jan. 2003, pp 256-269.

[13] C.T. Choi and C.K. Li, "Large signal modeling of quasi-resonant converters using regulated unified model," *Computers in Power Electronics, 200,. The 7th Workshop,* July 2000, pp. 132-138.

[14] A.F. Witulski, "Comparison of buck converter small signal dynamics pulse width modulated and quasi-resonant switches," *Applied Power Electronics Conference and Exposition, 1990. APEC'90, Conference Proceedings 1990, Fifth Annual,* 1990, pp. 195-204.

[15] S. Lungu, O. Pop and G. Chindris, "Educational platform for modeling of zero-voltage switching quasi-resonant boost converter," *Electronics Technology: Meeting the Challenges of Electronics Technology Progress, 2004., 27th International spring Seminar,* vol. 1, May 2004, pp. 147-152.

[16] B.T. Lin and Y.S. Lee, "A unified approach to modeling, synthesizing, and analyzing quasi-resonant converters," *Power Electronics, IEEE Transactions,* vol. 12, issue 6, Nov. 1997, pp. 983-992.

[17] K.T. Chau and A. Ionovic, "Small-signal model of quasi-resonant converters in the presence of conduction losses," *Circuits and Systems1 1991., IEEE International Symposium,* June 1991, pp. 1081-1084.

[18] C.C. Chong, C.Y. Chan and C.F. Foo, "A quasi-resonant converter-fed DC drive system," *Power Electronics and Applications, Fifth European Conference and Exposition, 1990. APEC '90. Conference Proceedings 1990., Fifth Annual,* March 1990, pp. 706-711.

[19] K. Yoshida, T. Ishi and N. Nagata, "Zero voltage switching approach for fly back converter," *INTELEC Conf. Proc.,* 1992, pp.324-329.

[20] K. Taniguchi, T. Yoshikawa, "Quasi-resonant PWM converter with high quality input waveforms and high efficiency," Proc. *IEEE PESC' 94,* 1994, pp. 1131-1136.

APPENDIX F
PRESENTATION SLIDES

Improvement study on soft-switched quasi-resonant DC/DC boost converter

UNIVERSITI
TEKNOLOGI
PETRONAS

Tran Minh Dung   4672

Supervisor: Mr. Nor Zaihar Yahaya

Table of Content

Abstract

❑ The project presents a new technique to reduce the soft-switched quasi-resonant boost converter losses

❑ Using active snubber circuit with an auxiliary switch and a clamp diode

❑ The energy from the inductor, which is in series with the main switch, after the auxiliary switch is turned off is returned to the input or delivered to the output by the active snubber

❑ Feasibility of the proposed circuit is verified by PSPICE simulation

Introduction

What ?

❑ Design a new circuit to improve the most recent study on soft-switched quasi-resonant DC/DC boost converter

Why ?

❑ Demand for soft-switched quasi-resonant DC/DC converters having high efficiency, small size and weight as well as low cost and high power operation

How ?

❑ Adding an active snubber circuit

Problem Statement

Recently, remarkable efforts have been made in soft-switched quasi-resonant DC/DC converters to reduce losses and increase switching frequency.

The current proposed circuit in Ba-Thunya and Prasad' s study using two coupled inductors and a clamp capacitor achieves high switching frequency and allows soft-switching

The main drawback is the voltage stress on the control switch and reverse-recovery-related losses of the boost rectifier at high switching frequencies.

The need of adding an active snubber circuit and a clamp diode to improve efficiency, reduce stress

---

Objectives and Scope of Work

Objectives

❏ To design an active snubber circuit consisting of an auxiliary switch in series with a clamp capacitor

❏ To simulate the design by PSPICE

❏ To evaluate the performance of the design

Scope of Work

❏ Consists of literature research on selected area, simulation of the design

❏ Make sure the performance meet the target of higher efficiency

Methodology

- ✓ Soft-switched Quasi-resonant DC/DC boost converter
- ✓ Snubber Network

Research

- ✓ Design Snubber Circuit
- ✓ Determine parameters
- ✓ Simulation in PSPICE

Design and Simulation

- ✓ Power efficiency
- ✓ Switch performance

Performance Analysis

Meet
Expectations ?

Technical Report
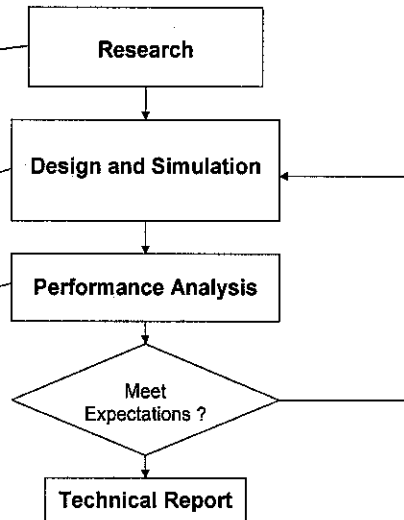
Result and Analysis

Original converter

Basic setting:

f_s = 167 kHz
T = 6 µs
V_{in} = 50 V
V_o = 60 V
D = 1/6

Lr1
27uH

Lr2
9uH

D1
MUR860

Cr1
0.1u

D2
BAL74

Cd1
1u

Rl
92

60
Vs1

M1
IRF843

D3
BAL74

Vpulse
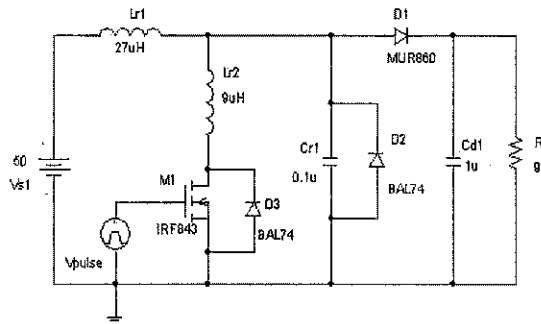
Original soft-switched quasi-resonant DC/DC boost converter

Main Switch – Power MOSFET (N-channel) type IRF843 (Rated 450 V, 250 KHz)
PER = 6 µs, PW = 1 µs, TD = 0, TF = 0, TR = 0, V1 = 0 V, V2 = 5 V
Boost rectifier, type MUR860 (Rated 600 V, 250 KHz)
Power diodes, type BAL74 (Rated 50 V, 250 KHz)

Result and Analysis

Modified converter

Clamp Diode
Minimize voltage stress on the rectifier

Active snubber
Reduce voltage stress on main switch, reduce reverse-recovery related losses of the rectifier

Modified soft-switched quasi-resonant DC/DC boost converter
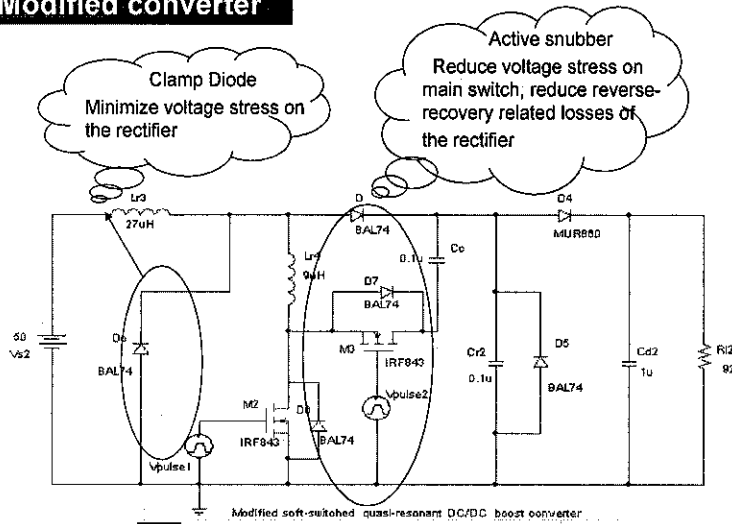
Result and Analysis

Switches setting

Main Switch – Power MOSFET
(N-channel) type IRF843
(Rated: 450 V, 250 KHz)
PER = 6μs, PW = 1μs,
TD = 0, TF = 0, TR = 0,
V1 = 0 V, V2 = 5V

Auxiliary switch – Power MOSFET
(N-channel) type IRF843
(Rated: 450 V, 250 KHz)
PER = 6 μs, PW = 4.5 μs,
TD = 1.3 μs, TF = 0, TR = 0,
V1 = 0 V, V2 = 5V

Calculation of snubber parameter

Based on the parameters in Ba-Thunya's original circuit:
$$L_s = 9\mu H, f_s = 167 KHz$$

Applying the resonance equation, the value of clamp capacitor can be determined

$$\omega_n C_o = \frac{1}{\omega_n L_s}$$

$$\omega_n = \frac{1}{\sqrt{L_s C_o}}$$

$$C_o = \frac{1}{(2\pi f_s)^2 L_s} = \frac{1}{(2\pi 167 k)^2 9\mu} = 0.1\mu F$$

Result and Analysis

Modified soft-switched quasi-resonant DC/DC boost converter

Result and Analysis

Operation modes

Mode 1 [T0, T1]

Mode 2 [T1, T2]

Mode 3 [T2, T3]

Mode 4 [T3, T4]
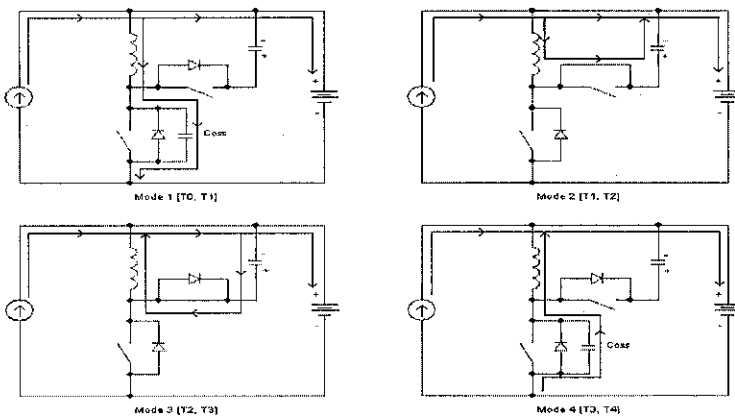
Result and Analysis
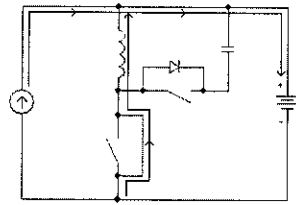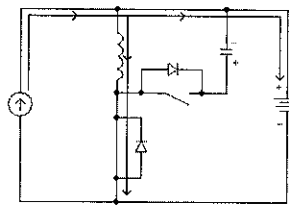
Mode 5 [T4, T5]   Mode 6 [T5, T6]
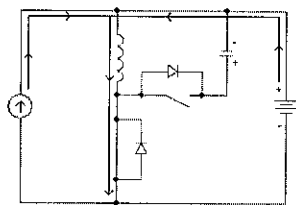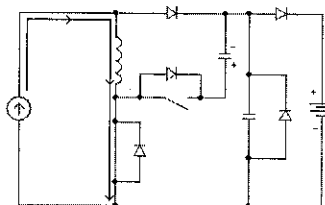
Mode 7 [T6, T7]   Mode 8 [T7, T8]

Result and Analysis

Output ripple voltage
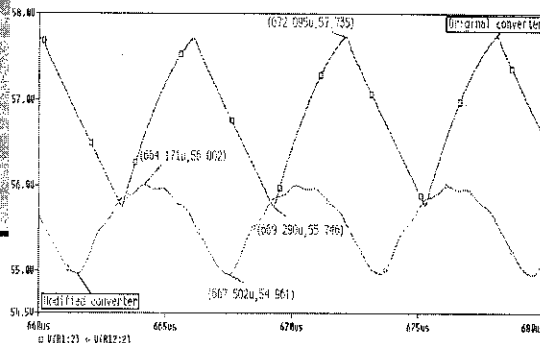
$$V_{o1(rip)} = \frac{56.0 - 54.9}{(56.0 + 54.9)/2} = 3.51\%$$

$$V_{o2(rip)} = \frac{57.7 - 55.7}{(57.7 + 55.7)/2} = 1.88\%$$

Result and Analysis

Power efficiency
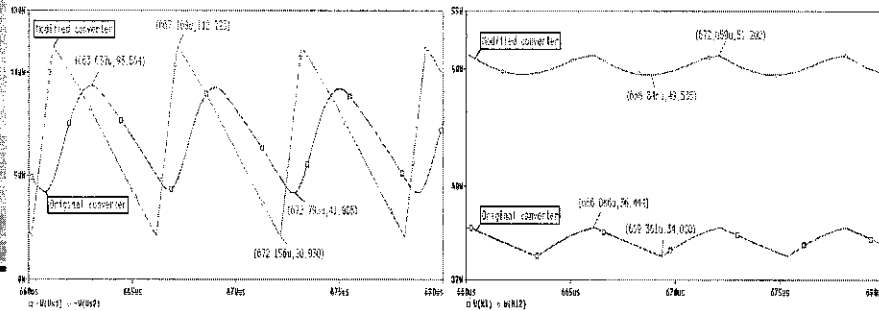
$$\eta_1 = \frac{P_{out1}}{P_{in1}} = \frac{W(R_1)}{W(V_{s1})} = \frac{35.5}{67.7} = 52.0\%$$

$$\eta_2 = \frac{P_{out2}}{P_{in2}} = \frac{W(R_{12})}{W(V_{s2})} = \frac{50.4}{66.6} = 75.6\%$$

Result and Analysis

V_{ds} of the main switch
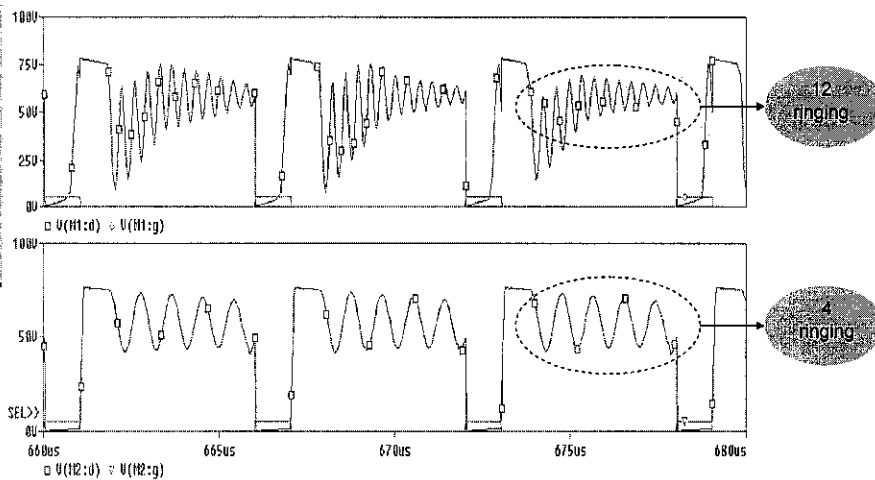
Result and Analysis

Waveform of switching power

(666.930u,320.270)

(666.031u,146.590)

Original converter

Modified converter

$P_{o1(peak)} = 320.3\ W$

$P_{o2(peak)} = 146.6\ W$
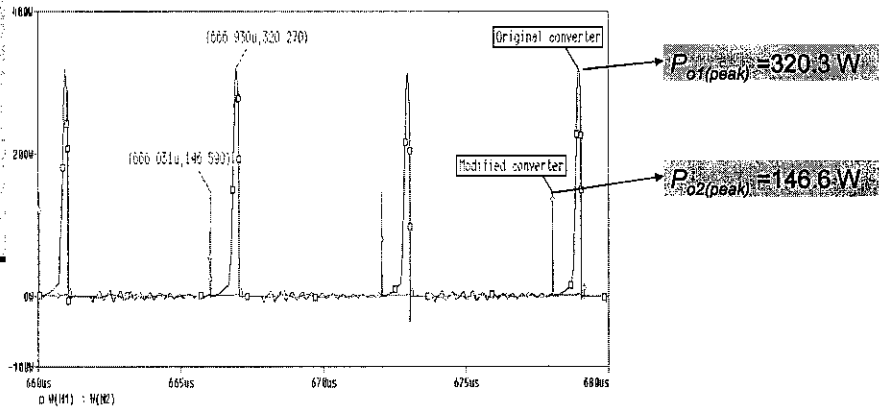
Result and Analysis

Boost rectifier voltage

Ringing

Ringing eliminated
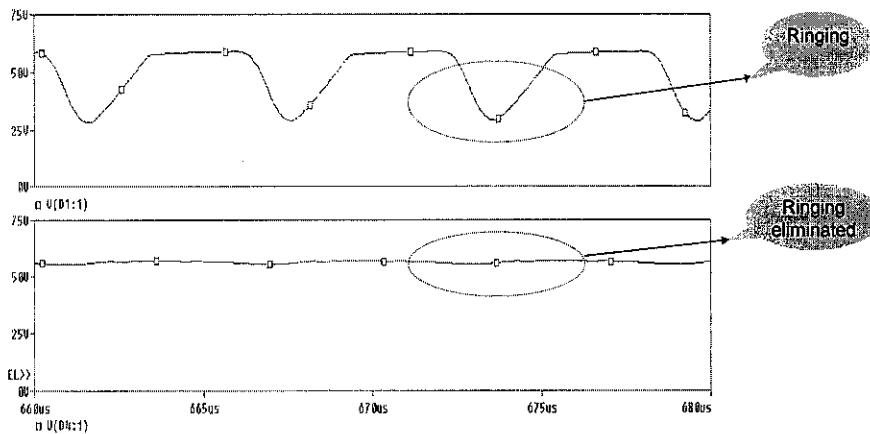
Result and Analysis

Criterion	Original boost converter	Proposed boost converter
Power efficiency	52.0%	75.6%
Output ripple voltage	3.51%	1.88%
Ringing on V_{ds}	12 components/period	4 components/period
Switching loss	Higher	Reduced
Ringing on rectifier voltage	Present	Eliminated
Number of components	9	14

Conclusion

❑ A novel soft-switched quasi-resonant DC/DC boost converter is proposed

❑ The technique employs an active snubber circuit with an auxiliary switch and a clamp diode to reduce losses in Ba-Thunya and Prasad 's original converter

❑ The proposed converter adopting this technique with input voltage of 50 V, 167 KHz switching frequency, duty ratio of 1/6 was simulated in PSPICE to verify the feasibility of the design

❑ Performance analysis of the proposed converter was done to validate the improvements to the original converter

1

Recommendation for Future Work

❑ Implement the PCB circuit

❑ Apply the technique to topology of other soft-switched quasi-resonant DC/DC converters

❑ Further study on the design with higher switching frequencies and higher voltage rating.

Question and Answer

Thank you!